SLAC PUB 3479
October 1984
(E/T)

Precision Measurement of the Total Cross Section for $e^+e^- \rightarrow$ *hadrons* at a Center of Mass Energy of 29 GeV*

E. Fernandez, W.T. Ford, N. Qi, A.L. Read, Jr., and J.G. Smith
Department of Physics, University of Colorado, Boulder Colorado, 80309

and

T. Camporesi, R. De Sangro, A. Marini, I. Peruzzi, M. Piccolo, and F. Ronga
Laboratori Nazionali Frascati dell'Istituo Nazionale di Fisica Nucleare, I-00044 Frascati, Rome, Italy

and

H.T. Blume, R.B. Hurst, J.C. Sleeman, J.P. Venuti, H.B. Wald, and Roy Weinstein
Department of Physics, University of Houston, Houston Texas 77004

and

H.R. Band, M.W. Gettner, G.P. Goderre, B. Gottschalk,[a] O.A. Meyer[b], H. Moromisato, W.D. Shambroom, and E. von Goeler
Department of Physics, Northeastern University, Boston Massachusetts 02115

and

W.W. Ash, G.B. Chadwick, S.H. Clearwater,[c] R.W. Coombes, H.S. Kaye,[d] K.H. Lau, R.E. Leedy, H.L. Lynch, R.L. Messner, S.J. Michalowski,[e] F. Muller, L.J. Moss, H.N. Nelson, K. Rich,[f] D.M. Ritson, L.J. Rosenberg, D.E. Wiser, and R.W. Zdarko
Department of Physics and Stanford Linear Accelerator, Stanford University, Stanford, California 94305

and

D.E. Groom, Hoyun Lee,[g] and E.C. Loh
Department of Physics, University of Utah, Salt Lake City, Utah 84112

and

M.C. Delfino, B.K. Heltsley[h], J.R. Johnson, T.L. Lavine, T. Maruyama, and R. Prepost
Department of Physics, University of Wisconsin, Madison Wisconsin 53706

Submitted to Physical Review D

* This work was supported in part by the Department of Energy, under contract numbers DE-AC02-81ER40025 (CU), DE-AC03-76SF00515 (SLAC), and DE-AC02-76ER-00881 (UW), and by the National Science Foundation under contract numbers NSF-PHY82-15133 (UH), NSF-PHY82-15413 and NSF-PHY82-15414 (NU), NSF-PHY80-06504 (UU), and by I.N.F.N. (Frascati).

Abstract

We report a high precision measurement of the ratio R of the total cross section for $e^+e^- \rightarrow hadrons$ to that for $e^+e^- \rightarrow \mu^+\mu^-$, at a center of mass energy of 29.0 GeV using the MAC detector. The result is $R = 3.96 \pm 0.09$. This value of R is used to determine a value of the strong coupling constant α_s of 0.23 ± 0.06, nearly independent of fragmentation models. Two different analysis methods having quite different event selection criteria have been used and the results are in agreement. Particular attention has been given to the study of systematic errors. New higher order QED calculations are used for the luminosity determination and the acceptance for hadrons.

PACS number: 13.65+i

Introduction

Precise knowledge of the total cross section for $e^+e^- \rightarrow hadrons$ is of fundamental importance to the understanding of the interactions of photons and partons. In particular the ratio of the cross section for producing hadrons to the cross section for producing point-like fermions like muons is one of the most important quantities in this understanding,

$$R = \frac{\sigma(e^+e^- \rightarrow hadrons)}{\sigma(e^+e^- \rightarrow \mu^+\mu^-)} .$$

The ratio R is expected to be nearly independent of the center of mass energy, $E_{c.m.}$, and given by the of quark flavors with a slowly varying correction due to QCD, and independent of the quark fragmentation process,

$$R = 3 \sum_{flavors} e_q^2 \times \left[1 + \frac{\alpha_s}{\pi} + 1.4\left(\frac{\alpha_s}{\pi}\right)^2 \ldots\right] ,$$

At $E_{c.m.} = 29$ GeV the effect of weak interactions on the hadronic cross section is approximately 0.2%. The factor 1.4 comes from a calculation in the $\overline{MS}$ renormalization scheme.[1-3] For five quark flavors, u, d, s, c, and b, having charges e_q in units of the electron charge, and a strong coupling constant $\alpha_s = 0.16$, one expects $R = 3.87$. (This value of α_s is more or less consistent with determinations from studies of event topology and energy-energy correlations in e^+e^- annihilation, and moment analysis of neutrino scattering experiments.[4-9]) QCD is able to predict not only the total cross section, but also the angular distribution of the thrust axis. This means that a powerful test of QCD also may be made over a restricted angular range.

The best published measurements of R have been primarily limited by systematic errors of 3 to 5%;[10-13] the statistical errors have been smaller. The systematic errors have generally been limited by uncertainties in acceptance calculations (model dependence), backgrounds (mainly two-photon interactions), and by radiative corrections (beyond α^3 effects). This experiment offers two different methods of event selection, one (Method A) relying heavily on calorimetry and having very large acceptance minimizing uncertainties in detection efficiency, and the other (Method B) relying heavily on charged particle tracking and using smaller angular acceptance to minimize background uncertainties. The two methods yield results which are compatible. The agreement of these complementary methods gives confidence in the acceptance calculations and the background estimates. This experiment also makes use of new higher order calculations of radiative corrections, which have not been considered by previous experiments.

Apparatus

The results are based on a sample of hadronic events collected at a center of mass energy of 29 GeV using the PEP e^+e^- storage ring and the MAC detector,[14–15] which is a general purpose device featuring 97% solid angle coverage with charged particle tracking as well as segmented total absorption electromagnetic and hadronic calorimetry. Figure 1 shows a schematic view of the MAC detector.

Detector

Charged particles are tracked in a cylindrical drift chamber surrounding the storage ring beam pipe. The chamber consists of ten cylindrical layers of drift cells at equally spaced radii from 12 to 45 cm in a common gas volume. Each cell is made up of a rectangular array of field wires centered on a closely-spaced pair of sense wires (to avoid left-right ambiguity), and layers of cells skewed at $\pm$ 3° stereo angles are interspersed with axial layers to allow measurement of the polar angle of the track. The chamber is inside a 2.3 m long, 50 cm radius, 7.5 cm thick aluminum solenoid coil, which provides an axial magnetic field of 0.57 T. The average position resolution of a drift cell is approximately 200 μm, resulting in a resolution in 1/momentum of $\sigma(1/p) = 0.065 \sin\theta$ (GeV/c)$^{-1}$ for polar angles in the range $23° < \theta < 157°$, where a track traverses all ten layers. The inner wall of the chamber plus the aluminum beam pipe comprise 0.036 radiation lengths at normal incidence.

The central drift chamber and solenoid coil are surrounded by a hexagonal barrel of electromagnetic calorimeter modules (shower chambers). Each of the six modules consists of 32 flat sheets of a lead-antimony-tin alloy 0.25 cm thick alternated with extruded aluminum proportional wire chambers, oriented with wires parallel to the beam. The 40 μm thick stainless steel anode wires are connected together in groups for

signal readout, such that each sextant is segmented in depth into three layers, each with 32 groups subtending equal azimuthal angles (about 1.9°). Each wire group is read out at both ends with low-impedance amplifiers, allowing measurement of axial position from charge division on the resistive wires. Each module comprises a total material thickness of 14 radiation lengths at normal incidence (including the coil as radiator for the first layer of chambers). The measured calorimetric energy resolution for electromagnetic showers is approximately $\sigma(E) = 0.20\sqrt{E\ (\mathrm{GeV})}$, while azimuthal and polar angular shower positions are measured with resolutions of 0.8° and 1.3°, respectively.

The central shower chambers are surrounded by a hexagonal hadron calorimeter of similar readout and construction, except that the thin lead alloy plates are replaced by steel. There are 24 layers with 2.5 cm thick plates followed by 3 layers 10 cm thick, for a total of about 5.8 nuclear interaction lengths of steel plus aluminum chambers at normal incidence (the electromagnetic calorimeter plus the solenoid coil add approximately 0.9 interaction lengths). This barrel is closed by planar endcaps consisting of 28 steel plates 2.5 cm thick followed by 2 layers of 10 cm thickness, also interleaved with proportional wire chambers. The hadronic energy resolution of this system, as measured in a test beam with pions of known momentum, is approximately described by $\sigma(E) = 0.75\sqrt{E\ (\mathrm{GeV})}$ for typical PEP particle energies. Polar angles are measured with a resolution of about 2°, and azimuthal angles to about 1° in the barrel and 4° in the endcaps. The first 9 layers of the endcaps have the chamber readout segmented more finely in the region that covers the ends of the barrel electromagnetic calorimeter. This part measures electromagnetic shower energies with a resolution $\sigma(E) = 0.45\sqrt{E\ (\mathrm{GeV})}$, with polar and azimuthal angular resolutions for showers of about 1.5° and 2°, respectively.

The central and endcap calorimeter steel is magnetized toroidally to a field of about 1.7 T, and is surrounded on all sides by 3 to 6 layers of drift chambers to track emerging charged particles. This system measures the momentum of emerging muons with a resolution of $\sigma(p)/p = 0.30$ (multiple scattering limited). In addition, there is a plane of scintillation counters after the innermost three steel plates in each central calorimeter sextant and after five plates in each endcap. These are used to form triggers and provide timing information for rejection of cosmic rays.

Event Trigger

Four independent triggers are employed for acquiring multi-hadron events, T_1, T_2, T_3, and T_4. Trigger T_1 selects events depositing substantial calorimetric energy over a wide range of angles or depth; to reduce cosmic rays grazing the outer calorimeter, scintillation counter signals are required with the hadron calorimeter signals. The trigger T_1 requires at least 2 of the set of 9 members {a central shower sextant having at least 1.5 GeV (6 members), at least 2.8 GeV deposited in an endcap calorimeter and at least one of the 4 scintillator quadrants at the same end (2 members), at least 4 GeV deposited in the entire central hadron calorimeter and at least one central scintillator}.

Triggers T_2 and T_3 both use the hits in the central drift chamber to make crude track definitions. For this purpose the central drift chamber is divided azimuthally into 18 overlapping wedges. Large angle wedges are designed to detect charged particles having an angle $\theta > 25°$, and thus traversing at least 8 layers of the central drift chamber. Such a wedge is "true" if at least three of the innermost five layers of the chamber and at least three in the outermost five layers contain hits. Similarly, 18 small angle wedges seek charged particles in the angular range $15° \leq \theta \leq 25°$, where only 3 to 7 drift chamber hits are expected. Such a wedge is "true" if 3 of the innermost 5

layers contain hits, and the corresponding large angle wedge is "false". The T_2 trigger is designed to detect two-photon annihilation events and seeks at least 2 well separated tracks and some minimal deposition of electromagnetic energy in the entire detector. T_2 is satisfied if there are at least 2 large angle wedges satisfied which are separated by at least 4 wedges, corresponding to about 90° in azimuth, and at least 0.5 GeV was deposited in each of two shower sextants (6 north, 6 south, and 6 central). T_3 seeks events having at least one charged particle reaching the scintillation counters and depositing minimum ionization energy in the hadron part of the calorimeter. T_3 is satisfied if there is at least one wedge, either large angle or small angle, having an associated scintillator and an associated hadron calorimeter signal at least 1/4 that of a minimum ionizing particle.

Trigger T_4 seeks events having at least two particles roughly coplanar with the beam direction and penetrating to the scintillation counters. T_4 is satisfied if at least 1 of the 3 opposite pairs of central scintillator sextants are hit, or any of the 4 pairs of opposite endcap scintillator quadrants (north with south) are hit, or at least 3 of the set of 8 members {a central scintillator sextant (6 members), the logical OR of the 4 north endcap scintillator quadrants, the logical OR of the 4 south endcap scintillator quadrants} are hit.

By making use of the overlap of event samples selected by these four triggers the inefficiencies of the triggers may be determined. Such a check will be sensitive to hardware failures which are not common to all the triggers; to the extent that any given trigger has no absolute losses of real events (expected to be the case) the overall trigger efficiencies may be determined. Using a sample of events determined to be multi-hadrons in later analysis the inefficiencies for $T_1 - T_4$ individually are 1.3, 1.1, 5.2, and $\overline{10.0}\%$ respectively. Since the triggers are used in a logical OR for accepting events, the

overall trigger efficiency is very high. All four triggers were satisfied on 84.6% of the events; three or more on 97.5%; and two or more on 99.6%. Monte Carlo simulations of the detector indicate that the efficiency for one or more trigger being satisfied is about 99.97%. A systematic error of 0.2% is assigned for this efficiency.

Charged Particle Tracking

The requirements on track selection are slightly different for the two analysis methods presented. For Method A acceptable tracks must have at least 5 out of the maximum of 10 points on the track, tracks having only 5 hits must have a momentum of at least 0.3 GeV/c, and there must be a primary vertex consistent with the nominal interaction point within reconstruction resolution. (Not all accepted tracks need come from this primary vertex.) For Method B greater reliance upon the quality of the tracking is required, so acceptable tracks must have at least 6 points, unless the reconstructed momentum exceeds 1 GeV/c, in which case at least 5 points are required. In addition, an acceptable event must contain at least one track having at least 7 points. All accepted tracks must be consistent with a common origin placed at the nominal interaction point.

Calorimeter Calibration

The accurate conversion of raw calorimeter pulse height into absolute energy deposition is essential to the interpretation of the detector response. This calibration must account for the fluctuating mix of photons and hadrons in hadronic events as well as the smaller fraction of detectable ionization resulting from hadronic cascades than from electromagnetic showers. The conversion constants for the three different absorber/proportional chamber systems (central shower, central hadron, and endcap calorimeters) are determined by a fitting procedure on real hadron events: The total

energy is required to have a mean near $2E_{Beam}$ independent of the thrust angle, and the width of the distribution is minimized. The resulting constants are consistent with those expected from extensive tests on prototype modules in a test beam[16] and the response of the calorimeters to Bhabha scattering events and minimum ionizing particles such as cosmic rays and muons. A similar procedure calibrates the Monte Carlo simulation (see Appendix I).

Luminosity Measurement

One of the major limitations in a precision measurement of R is the measured luminosity associated with the experiment. Several different methods have been employed to measure the luminosity for this experiment in order to study possible systematic errors.

Luminosity Monitor

Small angle Bhabha scattering may be used as one of the means of measuring the luminosity. Since the momentum transfers involved are quite small, $q^2 \approx -0.2$ (GeV/c)^2, the QED cross section is well understood. The luminosity monitor[17] consists of four identical scintillator/shower counter telescopes. Ordered from the interaction region each telescope consists of three scintillation counters, A, B, and C, 6 mm thick, and a shower counter S, 16 radiation lengths thick having 15 layers each of 13 mm scintillator and 6 mm lead. These counters are 32.6, 31.6, 57.0, and 95.3 mm square respectively. Two pairs of telescopes are positioned symmetrically about the interaction point in the horizontal plane at a distance of 4.72 m from the interaction point to counter B; the center of each telescope is at a scattering angle of 30 mrad. An acceptable Bhabha scattering event consists of the coincidence $(ABCS)_{NE} \cdot (CS)_{SW}$ using the north-east and south-west telescopes *etc.*; all four possible such combinations are recorded. A shower signal means at least 80% of the beam energy was deposited in each shower counter. By using the small counters on only one side of the coincidence, small departures are allowed from perfect back-to-back topology caused by radiative corrections, misalignments of the beam or the counter telescopes, and bending of the trajectories in the magnetic field.

Various sources of backgrounds have been studied; the contributions of these sources are summarized in Table 1. The largest background is due to beam pipe scattering,

in which a normal Bhabha scattering event, nominally at an angle smaller than the acceptance, scatters or showers in the shielding masks, sending by-products into the telescopes. The magnitude of this background can be estimated from the low energy tail of the shower counter pulse height. In addition the background has been computed by Monte Carlo techniques using the EGS[18] program for the showers. A closely related background comes from "backsplash" into the telescope, in which an electron misses the aperture defining counter, but where the by-products of the electromagnetic shower strike the defining counter. This effect has also been computed using the EGS program. A much smaller source involves a primary electron striking the shower counter and secondary particles from a photon from the primary vertex which converted in the beam pipe striking the defining counter; this has been computed by means of the Berends and Kleiss QED program[19] and EGS. Chance coincidences have been measured by running parallel electronic logic in which coincidences delayed by one revolution time were measured.

Table 1

Sources of Backgrounds in Luminosity Monitor

in % of Final Sample

Beam pipe scattering	1.5 ± 1.5
Backsplash into telescope	1.4 ± 0.5
Photon conversion in pipe	0.3 ± 0.1
Chance coincidences	0.2 ± 0.1
Total	3.4 ± 1.6

The precision of luminosity determination with the luminosity monitor is entirely limited by systematics. The symmetric disposition of the telescopes about the interaction point means that the sum of the four coincidence rates is independent of misalignments of the beam both transversely and longitudinally to first order in the displacements. In addition the four separate rates are recorded, and from the differences in the rates a correction may be made for misalignments. Typically the asymmetries are less than 5%, meaning a correction of less than 0.5%. Single counter efficiencies have been estimated by changes in the observed rates with respect to changes in thresholds; the overall system efficiency is estimated to be $99.0 \pm 1.0\%$. The energy cut on each shower counter of 80% of the beam energy is made off-line (the on-line trigger required only 40% of the beam energy). Imprecision in the energy calibration of the counters is estimated to contribute a 1.3% uncertainty in the luminosity determination. Radiative corrections are discussed in Appendices I and II. Table 2 summarizes the estimated systematic errors associated with the luminosity monitor.

Table 2

Estimated Systematic Errors for Luminosity Monitor

in % of Final Sample

Alignment	2.0
Backgrounds	1.6
Radiative Corrections	1.5
Energy Calibration	1.3
Counter efficiencies	1.0
Total	3.4

The luminosity determined from the luminosity monitor is 81.2 ± 2.7 pb^{-1}.

Central Bhabha Scattering

Large angle Bhabha scattering in the central detector may be used as a high precision monitor of luminosity. By using the main detector several kinds of systematic errors may be avoided: Inefficiencies in data recording and several kinds of detector failures will affect the hadron events and the central Bhabha scattering events in the same way; in such cases the resulting value of R is unchanged. The method naturally assumes the validity of QED for momentum transfer squared, $q^2 \approx -60$ (GeV/c)^2; tests to date indicate no departure of observations from QED, corrected for weak interaction effects.

The trigger for Bhabha scattering events is included in the event trigger previously described. The event candidates for Bhabha scattering are selected according to the following criteria:[20]

1. At least 2 and at most 3 tracks must be found in the drift chamber. At most one of these tracks found is allowed to miss the interaction region. About 96% of the events have exactly two tracks.
2. If a third track is found, exactly one of the tracks must be weak, that is it has fewer than 5 (out of a maximum of 10) hits in the drift chamber, or it has a momentum less than 0.5 GeV, or the third track must lie within 5° of another track.
3. The two main tracks are required to be collinear within 10°.
4. At least one of the two main tracks must satisfy $|\cos\theta| \leq 0.90$.
5. For events having both tracks within $|\cos\theta| \leq 0.80$ the total calorimeter energy is required to be at least half of the center of mass energy, *i.e.* $E_{cal} \geq 0.5 E_{c.m.}$.
6. Events having one or more tracks with $|\cos\theta| > 0.8$ need satisfy no specific

requirement on the total observed energy but rather are required to have at least 70% of the observed energy in the electromagnetic shower system.

The trigger efficiency is estimated to be $(99.8 \pm 0.1)\%$ by using the redundancy between the total energy trigger and the scintillation counter trigger. There is an inefficiency of $(2.0 \pm 0.5)\%$ in the energy selection criteria due to the gaps between the sextants of the calorimeter. The inefficiency due to the track reconstruction is estimated to be $(3 \pm 1)\%$ by hand scanning events satisfying the criteria used for selecting $\gamma\gamma$ events, described in the next section.

Two kinds of backgrounds were considered, $e^+e^- \rightarrow \tau^+\tau^-$ and $e^+e^- \rightarrow e^+e^-e^+e^-$. Events of these types were simulated by Monte Carlo programs and passed through the full detector simulation program. The $\tau^+\tau^-$ background as a function of θ is at worst only 0.2% and the $e^+e^-e^+e^-$ background is at worst 0.6%. Averaged over the whole angular range the combined backgrounds are only 0.2%. We assign a systematic error of 0.2% to the luminosity due to uncertainties in backgrounds.

Radiative corrections are made using the Berends and Kleiss program.[19] We assign an error of 0.4% for uncertainties in the radiative corrections.

The corrected luminosity is stable with respect to changing the cut on the acollinearity angle. Table 3 shows the relative change of the luminosity with respect to that obtained from the nominal cuts as a function of the cut on the acollinearity angle.

Table 3

Relative Change of Luminosity as a Function of Cuts on Acollinearity Angle

Central region	
6°	1.003 $\pm$ 0.002
10°	1.0
14°	0.993 $\pm$ 0.001
End cap region	
6°	0.994 $\pm$ 0.001
10°	1.0
14°	1.005 $\pm$ 0.001

We assign a systematic error of 1.0% on the luminosity due to the acollinearity cut.

The angular distribution is in good agreement with QED plus small corrections ($\leq$ 2%) due to weak interactions. The χ^2 is 8.3 for 8 degrees of freedom.

Table 4 summarizes the uncertainties in the measured luminosity.

Table 4

Estimated Systematic Errors for Central Bhabha Scattering

Track reconstruction	1.0 %
Acollinearity cut	1.0 %
Energy cut	0.5 %
Radiative Corrections	0.4 %
Backgrounds	0.2 %
Trigger efficiency	0.1 %
Total	1.6 %

The luminosity as determined from these Bhabha scattering events is 76.7 $\pm$ 1.2 pb^{-1}.

Photon Pair Production

The process $e^+e^- \rightarrow \gamma\gamma$ is another QED process which may be used for normalization purposes. It makes different assumptions on the validity of QED from the other methods. In particular it is nearly independent of modifications of the photon propagator (vacuum polarization), so it provides a cross check on the computation of QED cross sections. The process also allows tests of instrumentation.

The trigger is essentially the same as that used for Bhabha scattering events. The events are selected[20] by the following criteria:

1. No charged tracks pointing towards the origin are found in the central drift chamber.
2. At least 70% of the calorimeter energy appears in the electromagnetic part.

3. The thrust axis is required to be more than 30° from the beam axis to assure high track finding efficiency.
4. There are at least 2 and at most 5 clusters of hits in the shower system.
5. The two clusters having the highest energy (called primary clusters) must contain at least 90% of the shower energy.
6. The primary clusters are collinear within 10°, assuming that they originate from the interaction point.

No explicit requirement on the total energy is made.

The overall efficiency for acquiring these events is high. The trigger efficiency has been estimated to be 99.3% by use of a subset of the data having a looser trigger. The software efficiency for the first 3 selection criteria is 95% for $|\cos\theta_T| \leq 0.7$ and decreases to about 40% at $|\cos\theta_T| = 0.87$ due mainly to the selection on angle. (The angle the thrust axis makes with respect to the beam axis is θ_T.) The software efficiency is estimated by Monte Carlo techniques.

Three classes of backgrounds have been considered and found to be quite small. The dominant background is from Bhabha scattering events in which both tracks have been lost. By means of visual scanning a subset of the events it is estimated that about 0.4% of the events called $\gamma\gamma$ states are really Bhabha scattering events. Cosmic rays may shower in the outer part of the detector and in rare instances mimic a $\gamma\gamma$ event. By scanning events having some hits in the outer muon chambers we estimate that this background is about 0.1%. Since no explicit minimum energy deposition is required it is possible that random hits in the calorimeter could generate false events. The effect of random noise or other defects in the calorimeter is estimated to be about 0.1% by examining the ϕ distribution of events having a total energy less than 14.5 GeV. Only 1.4% of the entire sample has such low energy, and 90% of these low energy events lie

near the dead regions of the calorimeter.

Detailed comparisons have been made between the data and Monte Carlo generated events using the Berends and Kleiss program.[21] The angular distribution in the range $\theta \geq 35°$, after correction for detection efficiency and backgrounds, is in good agreement with that expected for QED, having a χ^2 of 7.8 for 10 degrees of freedom. The luminosity obtained from these events is stable with respect to changes in the cuts. Table 5 shows the relative change of the luminosity as a function of three of the cuts, changed one at a time; in all cases the number of clusters was required to lie in the closed interval 2 to 5. The results are normalized to that of the nominal cuts.

Table 5

Relative Change of Luminosity

as a Function of Cuts.

E_{shower}/E_{total}	
> 0.6	1.000 ± 0.001
> 0.7	1.0
> 0.8	0.999 ± 0.001
$E_{Primary\ clusters}$	
> 0.700	1.020 ± 0.001
> 0.900	1.0
> 0.975	1.000 ± 0.001
Acollinearity angle	
$< 6°$	0.994 ± 0.002
$< 10°$	1.0
$< 14°$	1.001 ± 0.003

There is some variation of the result with respect to changes in the energy required to be in the primary clusters. This is due to the difficulties in precisely modeling the detector; a systematic error of 0.5% is assigned to cover such uncertainties. The variation with respect to the collinearity angle cut is the same variation seen in Bhabha scattering. A small analytical correction, about 0.4%, has been made for the acollinearity distribution variations, but it has not been used in the overall luminosity determination. An uncertainty of 1% is assigned to this effect. The total uncertainty on detector modeling is 1.2%.

Table 6 summarizes the uncertainties in the measured luminosity.

Table 6

Uncertainties in Measured $\gamma\gamma$ Luminosity

Source	Uncertainty	
Detector modeling	1.2	%
Software Efficiency	0.5	%
Trigger Efficiency	0.2	%
Backgrounds	0.2	%
Radiative Corrections	1.0	%
Total	1.7	%

The luminosity as determined from the γ-pair final state is 77.9 ± 1.3 pb^{-1}.

Muon Pair Production

Mu-pair production is another process which may be used for normalization purposes; to do so requires assuming the validity of QED at large momentum transfers,

$q^2 \approx 900$ (GeV/c)^2. A sample of mu-pair events has been selected for the purposes of normalization; the selection criteria were essentially the same as previously published.[23] Briefly, events were required to satisfy the following criteria:

1. Exactly two tracks passing through the nominal interaction point are reconstructed in the drift chamber.

2. Each track has a polar angle satisfying $|\cos\theta| \leq 0.95$.

3. The tracks are required to be collinear to within 10°.

4. The sum of the energies of the two tracks must exceed 8 GeV.

5. Muons were identified by minimum ionization deposition in the calorimeters or by the presence of a matching track in the outer drift chambers; both members of the pair had to be identified as a muon for the event to be accepted.

As a test of the selection criteria, a more restrictive sample derived from the previous one is obtained by requiring $|\cos\theta| \leq 0.70$ and where tracks are rejected if the azimuthal angle ϕ lies within $\pm$ 2.5° of the six sextant boundaries. After acceptance and radiative corrections[22] the luminosity determined by the two different selection criteria agree within 0.2%.

Table 7 summarizes the background contributions, and Table 8 summarizes the systematic uncertainties in the μ-pair sample.

Table 7

Sources of Backgrounds in μ-pair Sample

in % of Final Sample

τ Decays	0.8
$ee\mu\mu$	0.3
Bhabha Scattering	$<$0.3
Total	1.1

Table 8

Estimated Systematic Errors for μ-pair Production

in % of Final Sample

Event Selection	2.0
Trigger	1.1
Radiative Corrections	0.4
Total	2.3

The luminosity as determined from the μ-pair final state is 75.5 ± 1.7 pb^{-1}.

Summary of Luminosity Measurements

Table 9 summarizes the integrated luminosity for the running period using the different methods.

Table 9

Summary of Integrated Luminosity in pb^{-1}

Method	Luminosity	Estimated Error
Luminosity Monitor	81.2	2.7
Detector Bhabha Scattering	76.7	1.2
γ-pairs	77.9	1.3
μ-pairs	75.5	1.7
Weighted mean of methods	77.1	1.2

The χ^2 for the hypothesis that all measurements of the luminosity are compatible is 3.8 for 3 degrees of freedom assuming all measurements are independent; the error computed on the weighted mean is 1.0%. Because of possible correlations we have chosen to use an error of 1.6%, which is the smallest error of the individual entries.

Hadron Event Selection Method A

Selection Criteria

One of the primary limitations of previous experiments' precision in measuring the total cross section is the uncertainty in the absolute detection efficiency. This uncertainty may be made very small by making the acceptance very large. In particular one wishes to accept events over the largest practical solid angle. Later selection criteria must use the available information to reduce the backgrounds to low levels. One must deal with several kinds of events:

1. The one-photon annihilation events sought are characterized by having a total energy in the final state equaling the sum of the two beam energies, and a total momentum of zero; very few competing background processes share these characteristics. (Initial state radiation has a modest effect, and corrections must be made.)
2. Two-photon annihilation events, *i.e.* $e^+e^- \rightarrow e^+e^-hadrons$, are usually characterized by (a) total energy of hadrons substantially lower than the available center of mass energy, (b) large missing momentum along the beam direction, (c) low momenta perpendicular to the beam line, and (d) relatively low charged multiplicity. A small fraction of these events will be essentially indistinguishable from one-photon annihilation events.
3. Tau pair events in which the τ's decay into multi-prong final states are a potential problem. The decay of one τ to one charged particle and the other to three charged particles takes place with a probability of about 25%, while the probability that both τ's decay into three or more particles is about 2%. Such decays of τ pairs are characterized by (a) low charged multiplicity, (b) missing energy

and momentum due to escaping neutrinos, and (c) tightly collimated jet(s) of low multiplicity.

4. Beam-gas interactions are characterized by a vertex at $x_0 = y_0 = 0$, but z_0 is uniformly distributed along the beam axis. In addition the total energy will be less than half the total center of mass energy, the missing momentum will be large, and the charged multiplicity will be low.

5. Cosmic-ray events are due to interactions of primary particles in the massive part of the detector. The secondary particles are usually small in number, and they rarely pass close to the nominal beam interaction point.

6. Bhabha scattering events which shower in the early part of the detector producing extra charged tracks may be confused with the multi-hadron events being sought. Such events are characterized by (a) a small number of tracks, (b) a large number of drift chamber hits not related to tracks, (c) a high electromagnetic energy density, and (d) small energy deposition in the hadron calorimeters.

Total energy, missing momentum (properly, missing directed energy), and energy density measurements are well matched to the use of calorimetry. For every element of energy deposited in the calorimeter, E_i, direction cosines c_x, c_y, and c_z are determined by lines connecting the interaction point and the position in the calorimeter. It is useful to define the visible energy E_v, the transverse energy E_t, the energy imbalance ratio I,

the energy deposited in the hadron part of the calorimeter E_h, and the average energy per calorimeter hit ρ,

$$\begin{aligned}
\vec{E}_i &= E_i \times (c_x, c_y, c_z) \ , \\
E_v &= \sum E_i \ , \\
E_t &= \sum E_i \sin\theta_i \ , \\
I &= |\sum \vec{E}_i| \, / E_v \ , \\
E_h &= \sum E_i(had) \ , \\
\rho &= E_v / N_h \ ,
\end{aligned}$$

where N_h is the number of hits in the calorimeter.

Information on charged particles is provided by the central drift chamber. Quantities dependent upon the charged particle tracking are the number of charged tracks N_{ch} (charged multiplicity), the vertex position, x_0, y_0, and z_0, and the sum of the magnitudes of the charged momenta,

$$P = \sum_{tracks} |\vec{p}_i| \ .$$

The event selection proceeds in two steps.[17] A loose set of cuts is applied to produce a good sample for further study. A second set of more stringent criteria is applied to the survivors. These cuts are summarized in Table 10.

Table 10

Event Selection Criteria for Method A

Quantity	Loose	Tight	
E_v	>12	>15	GeV
E_t	>7.5	>9.1	GeV
I	<0.65	<0.55	
E_h	no cut	>1.5	GeV
ρ	<1.1	<0.7	GeV
N_{ch}	≥ 5	≥ 5	
P	>2.0	>4.5	GeV/c
$\|z_0\|$	<5	<5	cm

Events passing all the tight cuts are accepted as multi-hadrons; events not passing all the loose cuts are regarded as either background or irretrievable multi-hadron events. Events between the tight and loose cuts have a high enough signal to noise ratio to warrant further investigation, and provide a sample of reasonable size for detailed visual scanning. In order to maximize acceptance we do not require that accepted events satisfy all the tight cuts. Events failing two or more of the tight cuts on E_v, E_t, or I, are rejected. Surviving events failing one or more of the tight cuts on any of the variables are examined visually, and are rejected if they are easily recognizable as a cosmic ray event, a radiative Bhabha scattering event, a τ-pair event, or a QED two-photon interaction event. Roughly 90% of the events passing the loose cuts also pass

the tight cuts. Of the 10% between the two sets of cuts, nearly all are classified as good events and retained as the result of the visual scan. (In the cases in which examination reveals some simple hardware failure, such as a dead part of the drift chamber leading to a reduced number of points on a track, caused the failure to pass the cuts, the event is retained.) The same scanning procedure has been applied to Monte Carlo events for multi-hadron events and simulations of background sources. These criteria result in a data sample of 36 642 events.

Acceptance

The detection efficiency for non-radiative events (*i.e.* in the hypothetical case that radiative corrections played no role) is about 0.93. This means that the selection criteria are such that a correction depending upon the physics input of the hadron production model is only about 7%, so that the uncertainty in this quantity is very low. Details on the model are given in Appendix I. Figures 2 (a) and (b) show the detection efficiency (the ratio of the number of events accepted to the number generated) as a function of (a) the radiated photon energy in units of the beam energy, and (b) the cosine of the thrust axis with respect to the beam direction. From these one sees that the primary losses are due to highly radiative events, with a small loss due to events whose jet axis lies very close to the beam direction. The overall acceptance $\mathcal{A}$ for real hadron events when radiative effects are considered is defined as the ratio of the accepted cross section, including losses due to pure instrumental effects and the effect of radiative corrections, to the lowest order cross section for point-like quarks. For the criteria used $\mathcal{A} = 1.113$, and it is greater than 1 because the observable cross section including higher order corrections is larger than the lowest order cross section. This comes about because (a) internal corrections raise the cross section by about 18% (vertex correction

= 8% and vacuum polarization = 10%) and (b) external corrections have two partially canceling contributions (hard initial state radiation lowers the center of mass energy of the eventual e^+e^- annihilation and thus increases the cross section; on the other hand the acceptance is decreased because of the lower energy and the missing momentum due to an escaping photon along the beam direction). Details on the radiative corrections may be found in Appendix II.

Backgrounds

The data selection criteria are sufficiently stringent that the backgrounds surviving these cuts are quite small; they are summarized in Table 11.

Table 11

Estimated Background Corrections in %

Two-Photon	
Hard Scattering	1.3 ± 0.5
VDM	1.0 ± 0.5
τ production	0.9 ± 0.2
Beam-gas	<0.2
Other sources	<0.2
Total	3.2 ± 0.7

The primary contribution is due to residual two-photon events. This contribution has been estimated by means of Monte Carlo methods, using a hard scattering model and a Vector Dominance Model (VDM) model. Details may be found in Appendix III. The hard scattering model for $e^+e^- \rightarrow e^+e^-q\bar{q}$ yields an estimated background of [1.3

$\pm$ 0.2 (statistical) $\pm$ 0.4 (systematic)]%. The Vector Dominance Model contribution has been estimated to be (1.0 $\pm$ 0.5)%, using input data on the total cross section for $\gamma\gamma \rightarrow$ *hadrons* from the PLUTO[24] collaboration and the TASSO[25] collaboration. The TASSO cross section is about 50% larger than the PLUTO cross section. Our own measurements (*cf.* next section) are in better agreement with the TASSO results than those of PLUTO, so we have used the larger cross section of TASSO, and assigned a 50% systematic error to the VDM calculation.

The τ decay contribution has been estimated to be (0.9 $\pm$ 0.2)% using the following branching ratios: $B(\tau \rightarrow 3\text{-}charged\ +\ neutrals) = (14.0 \pm 0.7 \pm 1.0)\%$,[26] and $B(\tau \rightarrow \geq 5 - charged\ +\ neutrals) < 0.7\%$. The events from τ-decay resulting in ≥ 5 prongs detected are partially due to events in which both τ's decay into three charged particles (0.5%) and partially due to photon conversion in lower multiplicity (1 + 3 prong topology) events (0.4%). The acceptance for such τ-pair events is about the same as that for hadron events.

Comparison of Data and Monte Carlo

The agreement between the Monte Carlo calculations and the observed distributions of physical variables is generally good. Figure 3 shows a comparison of data (points) and Monte Carlo calculations (histogram) for distributions of (a) E_v, (b) E_t, (c) I, (d) N_{ch}, (e) P, and (f) thrust angle. The Monte Carlo calculations include both one-photon events and two-photon events for direct comparison with the observations. Slight displacements between the data and the Monte Carlo plots are visible, but as will be shown the result for R is stable with respect to large changes in the cuts on these variables. Note in particular that there is good agreement of the distribution of the thrust axis angle; a residual contamination of two-photon events would show up at large values of $\cos\theta_T$.

The result is stable with respect to changes in the cuts. In particular, each of the variables E_v, E_t, I, N_{ch}, and P was varied, one at a time, from the values used in the loose cuts; the resulting value of R changed by no more than 1% from the standard value over the following ranges, $12 \leq E_v \leq 28$ GeV, $7.5 \leq E_t \leq 18$ GeV, $0.36 \leq I \leq 0.65$, $5 \leq N_{ch} \leq 8$, and $2 \leq P \leq 6$ GeV/c. As another test of sensitivity to cuts, events with three or four charged tracks and passing all the other loose cuts also have been analyzed. This low multiplicity sample has a very high contamination from τ-pairs, Bhabha events with extra tracks, and two-photon QED events such as $eeee$ or $ee\mu\mu$. Monte Carlo studies verified that visual scanning could effectively remove essentially all backgrounds along with about half of the real three or four prong multi-hadron events passing the loose cuts. Events with three or four prongs surviving the scanning constitute 1% of the total multi-hadron sample, in good agreement with the Monte Carlo estimate. These events are not included in the final sample, but they would not change R if they were.

We have tested the Monte Carlo modeling of the one-photon annihilation process as well as the backgrounds by loosening the cuts made to accept more events, especially those due to two-photon annihilation. Three sets of data were selected which fail the loose cuts described above but have $N_{ch} \geq 5$ and satisfy the following requirements:

Set I: $E_v > 11$ Gev, $E_t > 7$ GeV, and $I < 0.7$.

Set II: $E_v > 10$ Gev, $E_t > 6$ GeV, and $I < 0.8$.

Set III: $E_v > 8$ Gev, $E_t > 0$, and $I < 0.85$.

Table 12 summarizes the observed cross section and the expected contributions to the cross section for each data set. It also shows the change in R if the additional data had been accepted into the primary data sample.

Table 12

Sensitivity of R to Looser Cuts

	Set I	Set II	Set III	
Increase of data sample	6	12	26	%
Raw observed cross section	25.0	56.3	120.5	pb
Monte Carlo estimated cross sections				
One-Photon	11.5	22.2	33.5	pb
Two-Photon VDM	11.9	26.6	66.9	pb
Two-photon hard scatter	2.4	6.2	14.4	pb
Other background	1.0	1.5	4.8	pb
Unaccounted	–2.0	0.0	1.0	pb
Change in R	–0.4	0.0	0.2	%

The conclusion is that even if the cuts had been loosened to Set III, which increases the data sample by 26% (more than half of which is two-photon background), the value of R would not have changed significantly. Because of substantial experimental uncertainties in the VDM contribution we assign a 50% uncertainty in this contribution. (See Appendix III.) In view of the agreement in this extended sample, the assignment of a 50% error to the VDM calculation is conservative.

As a further test of the two-photon background subtraction the standard data sample is divided into three regions defined by the angle the thrust axis, as computed from the energy flow vectors, makes with respect to the beam axis, θ_t; the small angle data should contain a larger fraction of this background than the larger angle data. In each of these regions a value of R is determined, using the same criteria used for the whole

sample. Table 13 summarizes the results.

Table 13

Measurement of R in three angular regions

	$0° \leq \theta_t < 30°$	$30° \leq \theta_t < 55°$	$55° \leq \theta_t \leq 90°$	
Fraction of data	13	34	53	%
Hard scatt. $\gamma\gamma$ background	3.5	1.4	0.7	%
VDM $\gamma\gamma$ background	5.3	0.2	0.2	%
$(R_{region} - R_{whole})/R_{whole}$	0.9	–0.5	0.1	%

The stability of the results even in the presence of two-photon backgrounds as large as 8.8% in the small angle region indicate that these backgrounds have been well estimated.

The distribution of $\cos\theta_T$, shown in Fig. 3, has been fit to the form $dN/d\cos\theta = 1 + B\cos^2\theta$,after efficiency and radiative corrections, for the parameter B. The result is $B = 0.98 \pm 0.07$. This is consistent with the expected value of 1.0 for massless quarks, and slightly less for the realistic case.

Results

The resulting value for R for Method A is given by

$$R = \frac{N_e - N_b}{\mathcal{A}\mathcal{L}\sigma_{\mu\mu}} ,$$
$$= 4.00 \pm 0.03\ (statistical)\ \pm 0.09\ (systematic) ,$$

where N_e is the number of experimentally observed events, N_b is the estimated number of background events, $\mathcal{L}$ is the integrated luminosity, and $\sigma_{\mu\mu}$ is the mu-pair point-like cross section, $\sigma_{\mu\mu} = 4\pi\alpha^2/(3s)$. The quoted uncertainty is almost entirely systematic.

We have varied α_s in the Lund Monte Carlo program from 0.13 to 0.24 and find that the acceptance varies by about $\pm$ 0.5% from the value used. Instead of the string model, we have used the independent jet option in the Lund program, and find that the acceptance changes at most by 0.5% from the string result. Because of the large acceptance the result is rather insensitive to other parameters.

No significant time dependence of the data has been observed. The entire sample was divided into sets of about 4 pb^{-1} each, corresponding to about 2000 events. Mean values of E_v, E_t, N_{ch}, and the ratio of the luminosities as determined by the luminosity monitor and the μ-pairs to the main detector Bhabha scattering determination, and the value of R were computed. No significant time dependence of any of these quantities was seen.

Table 14 summarizes the uncertainties in the determination of R.

Table 14

Uncertainties in R in % for Method A

Quantity	Statistical	Systematic
Event sample		
Number of events	0.5	
Trigger and filter		0.2
Calorimeter gain stability		0.3
Acceptance		
Detector modeling	0.4	1.0
QCD and fragmentation		0.5
Radiative corrections		1.0
Backgrounds		
Two-photon		0.7
τ-pairs		0.3
Luminosity		1.6
All in quadrature	0.6	2.3

Hadron Event Selection Method B

Selection Criteria

Since two-photon and beam-gas interactions peak at small angles of the thrust axis with respect to the beam direction, eliminating events having small angles will preferentially remove these backgrounds. Two-photon events and beam-gas interactions also tend to have a smaller charged multiplicity and observed energy than the one-photon annihilation events. More restrictive event selection criteria than applied in the previous section will produce a purer sample of one-photon annihilation events at the expense of a larger acceptance correction. The criteria employed[27] are shown in Table 15.

Table 15

Event Selection Criteria for Method B

$$|\cos\theta_T^p| \leq 0.57$$
$$N_{ch} \geq 5$$
$$E_v \geq 16 \quad \text{GeV}$$

For the purpose of calculating the thrust direction, $\cos\theta_T^p$, only charged tracks were used.

These selection criteria result in a sample of 17 767 hadron event candidates.

Acceptance

The corrections for these cuts were done by Monte Carlo methods, which are similar to those discussed in the previous chapter. The acceptance $\mathcal{A}$, including radiative

corrections, is 0.564. The $\cos\theta_T^v$ cut removes about half of the one-photon annihilation events; the other two cuts remove only a few percent. Having made the Monte Carlo correction using the model as it comes from the event generator, the results were fine tuned with additional small corrections to the Monte Carlo distributions to agree with the observed distributions of variables used for the selection criteria. These adjustments are described in the section on comparison of the data and the Monte Carlo.

Backgrounds

The backgrounds in this data sample are very small, and are summarized in Table 16. As a check on the background estimates, a control data set having $8 \leq E_v < 16$ GeV was used.

Table 16

Estimated Background Contributions in %

Referred to One-Photon Annihilation

	$8 \leq E_v < 16$ GeV	$E_v \geq 16$ GeV
Observed	6.8	–
Estimates		
Two-photon (VDM)	4.5	0.0
Two-photon (hard scattering)	0.4	0.5
τ-pair production	0.1	0.4
Beam-gas	0.2	0.0
Other sources	0.6	0.1
Total estimate	5.8	1.0

The "observed" entry in the first column has been corrected for a small residual of one-photon annihilation events which lie within the cuts. The two-photon background was computed by Monte Carlo methods taking into account contributions from both a hard-scattering model and a Vector Dominance Model; see Appendix III. The τ-pair production background was also computed by Monte Carlo methods. The beam-gas contribution was estimated using the z_0 distribution of the event vertex. The remaining backgrounds considered were cosmic rays showering in the detector, multi-prong Bhabha scattering events, "beam-splash" events in which some off-axis beam associated particle struck the beam pipe, and events involving electrical breakdown in the detector. These sources were estimated by visually scanning a subset of the data.

Comparison of Data and Monte Carlo

Comparisons have been made between the data and Monte Carlo calculations by examining distributions of one variable at a time when the other variables are fixed at their nominal values.

The distribution of N_{ch} for the data is systematically lower than the corresponding distribution for the Monte Carlo events. The observed mean values for $N_{ch} \geq 5$ are 9.7 and 10.1 for data and Monte Carlo respectively. Multiplying the Monte Carlo distribution, treated as a continuous distribution, by the ratio of these two mean values brings the two distributions into good agreement. Figures 4a and 4b show the distribution of N_{ch} for the data and the Monte Carlo before and after the scaling of the Monte Carlo respectively. According to the Monte Carlo model, 4.3% of the one-photon annihilation events fail the N_{ch} cut; using the scaled Monte Carlo distribution instead of the original unscaled distribution lowers the acceptance by 1.0%. As a check on the Monte Carlo calculations the fraction of 4-prong events (which are rejected in the normal analysis)

was compared with the data. The events were required to satisfy all the other cuts of the normal analysis except that there be two tracks in each hemisphere with respect to the thrust axis. The topology requirement strongly suppresses two-photon annihilation and beam-gas interaction backgrounds, resulting in a nearly pure one-photon annihilation data sample. Events of this type are 0.4% of the normal sample, and 0.5% of the Monte Carlo sample, indicating that the modeling is good.

Figure 5 shows the distribution of E_v for the data, corrected for estimated backgrounds, and the Monte Carlo for $N_{ch} \geq 9$; this multiplicity cut provides a background-free sample for the comparison. The agreement between the data and the Monte Carlo is quite good. The Monte Carlo model indicates that 1.8% of the one-photon events fail the $E_v \geq 16$ GeV cut. Figure 6 shows the E_v distribution for the normal data sample, uncorrected for backgrounds, with Monte Carlo contributions from one-photon and two-photon annihilation.

Results

The value of R obtained from Method B is

$$R = 3.91 \pm 0.04\ (\textit{statistical}) \pm 0.10\ (\textit{systematic})\ ,$$

which is in good agreement with the result obtained by the other method. Since the two methods have different possible biases, the agreement gives one confidence in the estimated systematic errors.

This analysis assumes that the angular distribution of the jet axis is well known, and is given by QCD. Assuming only that the final state is the result of one-photon annihilation then the angular distribution of the jet axis must be of the form

$$\frac{d\sigma}{d\Omega} \propto 1 + B\cos^2\theta$$

where $|B| \leq 1$. In the context of the quark-parton model for massless quarks it is expected that $B = 1$. Massive quarks modify the value of B slightly, depending upon the center of mass energy; the Monte Carlo model takes this variation into account. The value of R is stable with respect to changing the cuts on $\cos\theta_T^p$. Table 17 shows the value of R after corrections for acceptance and backgrounds as a function of the cut made on $\cos\theta_T^p$, expressed as a ratio to the value at the nominal cut of 0.57; the quoted errors are statistical. We assign an error of 0.5% to R for uncertainties due to the angular cut.

The agreement of the value for R from this method and that of Method A may be used to determine the coefficient B in the angular distribution of the jet axis by using the ratio of the R values obtained by the two methods. The result is $B = 0.87 \pm 0.10$.

Table 17

Values of R Using Different Cuts on $\cos\theta_T^p$

Expressed as a Ratio to Nominal Cut Value

$\cos\theta_T^p \leq 0.4$	1.011	$\pm$ 0.012
$\cos\theta_T^p \leq 0.5$	1.004	$\pm$ 0.008
$\cos\theta_T^p \leq 0.6$	1.000	(ref)
$\cos\theta_T^p \leq 0.7$	0.997	$\pm$ 0.007
$\cos\theta_T^p \leq 0.8$	1.019	$\pm$ 0.009

The value of R is stable with respect to changes in the cut on N_{ch}. Table 18 shows the value of R after corrections for acceptance and backgrounds as a function of the cut made on N_{ch}, expressed as a ratio to the value at the nominal cut of 5. Because the contamination from τ-pairs changes abruptly below $N_{ch} = 5$, we do not attempt to evaluate R there with this method.

Table 18

Values of R Using Different Cuts on N_{ch}

Expressed as a Ratio to Nominal Cut Value

$N_{ch} \geq 5$	1.000 (ref)
$N_{ch} \geq 6$	0.998 $\pm$ 0.004
$N_{ch} \geq 7$	0.994 $\pm$ 0.005

The result is also stable with respect to changes in the cut on E_v. Table 19 shows the value of R after corrections for acceptance and backgrounds as a function of the cut made on E_v, expressed as a ratio to the value at the nominal cut of 16 GeV. The largest deviation is 0.9% at the lowest cut of 12 GeV. A subsample of events having $N_{ch} \geq 9$ and $E_v \leq 16$ GeV has been studied to check the modeling of the low energy tail. After background corrections we observe 1.5%, referred to the one-photon events, in this region for the data and 1.5% for the adjusted Monte Carlo. We assign a 0.8% error in R due to the E_v cut.

Table 19

Values of R Using Different Cuts on E_v

Expressed as a Ratio to Nominal Cut Value

$E_v \geq 12$ GeV	1.009 $\pm$ 0.003
$E_v \geq 14$ GeV	1.008 $\pm$ 0.002
$E_v \geq 16$ GeV	1.000 (ref)
$E_v \geq 18$ GeV	1.001 $\pm$ 0.002
$E_v \geq 20$ GeV	1.004 $\pm$ 0.003

Extensive checks have been made to test the possible dependence of the acceptance upon the parameterization of the hadronic event generation. Table 20 summarizes the variations of parameters and R. The range shows the lower limit, the nominal value, and the upper limit explored for the parameter. The range of parameters is that allowed by existing experiments. The changes in $\mathcal{A}$ with respect to the nominal value are in the same order as the values of the parameters. The quantity $P/(P+V)$ is the ratio of pseudoscalar to vector particles produced, which affects the charged multiplicity. The quantity σ_q is a measure of the transverse momentum distribution of mesons produced during the fragmentation. The fragmentation function for the c and b quarks has been varied. In addition to the Peterson function[28] with $\epsilon = 0.4$ and 0.04 for c and b quarks respectively, the fragmentation functions $1-z$ and *constant* were tried. T_{max} is a cut-off parameter on thrust used in the computation in deciding whether to generate a gluon or not. We assign a 1.1% error to R due to the QCD modeling.

Table 20

Changes in Acceptance due to Variations in Monte Carlo Parameters in %

Quantity	Range	$\delta\mathcal{A}$
$P/(P+V)$	0.35–0.50–0.65	+0.4 –0.4
α_s	0.12–0.17–0.22	+0.6 –0.4
σ_q	0.15–0.30–0.45 GeV/c	–0.3 +0.5
Fragmentation function	(see text)	$\pm$0.8
T_{max}	0.93–0.95–0.97	$\pm$0.1

The sources of systematic errors are summarized in Table 21.

Table 21

Uncertainties in R in % for Method B

Quantity	Statistical	Systematic
Event sample		
Number of events	0.8	
Trigger and filter		0.2
Acceptance		
Angular cut		0.5
Multiplicity cut		0.5
Energy cut		0.8
QCD and fragmentation		1.1
Radiative corrections		1.0
Backgrounds		
Two-photon		0.3
Others		0.3
Luminosity		1.6
All in quadrature	0.8	2.5

Summary and Conclusions

We have presented two precision measurements of the ratio R of the total cross section for $e^+e^- \rightarrow hadrons$ to that for $e^+e^- \rightarrow \mu^+\mu^-$ using two very different methods having different possible biases. Method A gives $R = 4.00 \pm 0.03 \pm 0.09$, and Method B gives $R = 3.91 \pm 0.04 \pm 0.10$. The two results agree with each other, and taking a simple mean our final result is

$$R = 3.96 \pm 0.03\ (statistical) \pm 0.09\ (systematic).$$

The systematic error on our final result has not been reduced below 0.09 because of possible correlations between the two methods.

The achievement of a systematic error of about 2% is the result of detailed study of acceptance and backgrounds. In addition the radiative corrections have been treated to all leading-logs for the first time. If radiative correction calculations only through α^3 are used the value of R increases by 1.1% to 4.00. Our measurement is in agreement with other measurements of R, shown in Table 22.

Table 22

Comparison of Recent R Measurements

R	Statistical Error	Systematic Error	Experiment
3.96	0.03	0.09	This experiment
3.97	0.05	0.10	JADE[13]
4.01	0.03	0.20	TASSO[10]
3.84		0.22	Mark J[11]
3.90		0.25	Mark II[12]

The resulting value of R is in agreement with the prediction of QCD, 3.87, using a value of $\alpha_s = 0.16$ as derived from other experiments[4–9]

$$R = 3 \sum_{flavors} e_q^2 \times \left[1 + \frac{\alpha_s}{\pi} + 1.4\left(\frac{\alpha_s}{\pi}\right)^2 \ldots\right],$$

using the $\overline{MS}$ renormalization scheme. Conversely, our value of R may be used to determine α_s; the result is 0.23 ± 0.06. While the absolute error of this determination is relatively large, it is essentially model independent.[29] In terms of the QCD scale parameter Λ

$$\alpha_s = \frac{12\pi}{(33 - 22n_f)\log(|q^2|/\Lambda^2)}$$

(to lowest order in $\log q^2$), where n_f is the number of quark flavors whose masses squared are small compared to $|q^2|$, we obtain a value $\Lambda = (0.82\ {}^{+0.90}_{-0.59})$ GeV^2, using five quark flavors.

There has been some controversy regarding the model dependence of the value of α_s determined by some of the existing methods,[30] such as energy flow, heavy quark-onia, and event topology in e^+e^- annihilation, and deep inelastic lepton scattering. Details of quark fragmentation and higher twist effects often enter in uncontrolled ways. In addition each process is only computed to a finite order in α_s, and the truncation errors in this perturbation series are variable from process to process and unknown. The relation between α_s and Λ is strictly only valid only when $|q^2|$ is large compared to the square of all quark masses. This can be a problem in using the decay rate of heavy quark-onia and lepton scattering. It is therefore not surprising that values of α_s and Λ vary considerably from process to process.

Acknowledgments

We should like to thank the PEP staff for the excellent operation of the PEP storage ring during the data taking. We are very grateful for the efforts of the engineers, technicians, and staff of the collaborating institutions in the construction and operation of the detector, and we should particularly like to acknowledge the contributions of D. Clark, J. Escalera, M. Frankowski, T. Pulliam, and J. Schroeder. The running of the MAC detector would have been much more difficult without their tireless efforts.

We should like to thank Dieter Freytag for his contributions to the MAC electronics and finally, we should like to acknowledge the contributions of Y.S. Tsai to our theoretical understanding of the higher order radiative corrections.

This work was supported in part by the Department of Energy, under contract numbers DE-AC02-81ER40025 (CU), DE-AC03-76SF00515 (SLAC), and DE-AC02-76ER00881 (UW), and by the National Science Foundation under contract numbers NSF-PHY82-15133 (UH), NSF-PHY82-15413 and NSF-PHY82-15414 (NU), NSF-PHY80-06504 (UU), and by I.N.F.N. (Frascati).

Appendix I Monte Carlo Modeling

The acceptance, $\mathcal{A}$, is defined as the ratio of the accepted, radiatively corrected cross section to the total point cross section for quark pair production. It is used to correct the data sample for the effects of QED radiation, detector performance, and the event selection procedure. The calculation of the acceptance was done by Monte Carlo means in which hadronic events were generated and the detector's response was simulated in a realistic way. A sample of Monte Carlo events representing 25 pb^{-1} of e-pair collisions was generated for the acceptance determination. This integrated luminosity corresponds to 13 318 $q\bar{q}\,(\gamma)$ states produced over all available phase space by the modified Berends-Kleiss-Jadach[45] $q\bar{q}\,(\gamma)$ Monte Carlo program.

Lowest Order Radiative Corrections

The event simulation begins with the generation of quark-antiquark pairs with weak-electromagnetic corrections. A modified version of the Berends, Kleiss, and Jadach program produces $q\bar{q}\,(\gamma)$ final states over all available phase space. The original program performs a similar task for muon pairs; alterations to handle the quark case consisted of the removal of terms involving final state radiation, insertion of fractional quark charge factors where applicable, and appropriate weak isospin assignments for the quarks. Fig. 7 shows the Feynman diagrams considered. The lowest order pure QED process (a) has α^3 contributions from not only its interference with the vertex graph (b), the vacuum polarization (c), and the box diagrams $(d)-(e)$, but also from the initial state bremsstrahlung of $(f)-(g)$ and their interference with each other. The corresponding graphs with Z^0 exchange in $(h)-(o)$ each contribute directly to the cross section as well as through the interference of $(j)-(m)$ with one another and $(a)-(e)$ and of $(n)-(o)$

with each other and $(f)-(g)$. The weak diagrams have been included for completeness, but at $E_{c.m.} = 29$ GeV contribute a negligible amount to the total cross section.

Because of the infrared divergence for low energy photons the $q\bar{q}(\gamma)$ event generator has a photon energy cutoff k_0, in units of the beam energy, (arbitrarily set at 0.01) below which no photons are generated. Since the integrated cross section below the cutoff is finite and such soft photon events are experimentally indistinguishable from photon-less events, this cross section is combined with that from lowest order with its virtual corrections. At the other end of the photon spectrum, a non-zero quark mass m_q introduces a kinematic maximum $k_{max} = 1-(m_q/E_{beam})^2$.

Factoring the acceptance $\mathcal{A}$ into two terms as $\mathcal{A} = \epsilon(1+\delta)$ isolates the roles of the overall efficiency ϵ, that fraction of the total radiatively corrected cross section passing the selection criteria, and the fractional change δ in the total cross section from radiative corrections. Table 23 summarizes the composition of the radiatively corrected total cross section, summed over all five quark flavors,

$$\sigma_{rc}(\text{total}) \equiv \sum_q \int_0^{k_{max}} \left(\frac{d\sigma}{dk}\right)_q dk$$

at $E_{c.m.} = 29$ GeV in terms of the vertex contribution, vacuum polarization, and bremsstrahlung above and below k_0. The hard bremsstrahlung contribution depends on the quark masses used (through k_{max}), namely, 0.3, 0.3, 0.5, 1.6, and 5.0 GeV/c^2 for flavors u, d, s, c, and b, respectively. The precise value of $(1+\delta)$ is not fundamental because quark masses are not precisely known. Slightly different choices for these masses do not significantly alter $\mathcal{A}$ because the efficiency for events with hard initial state radiation is very small; *cf.* Fig. 2. Any change in $(1+\delta)$ is accompanied by a nearly offsetting change in ϵ; hence the exact values of ϵ and δ are strongly dependent on the approach to handling hard photons, but the resulting value for $\mathcal{A}$ is not.

Table 23

Contributions to the Radiative Correction δ

Type of contribution		Contribution
Vertex correction		0.079
Vacuum polarization		0.100
(e-pairs)	0.031	
(μ-pairs)	0.015	
(τ-pairs)	0.006	
(*hadrons*)	0.048	
Bremsstrahlung		0.227
($k < 0.01$)	−0.447	
($k > 0.01$)	0.674	
Total		0.406

There is a number of uncertainties and model dependencies in the foregoing evaluation of $(1 + \delta)$:

(a) It represents a consistent calculation in QED to order α^3 only, ignoring higher order effects which increase the α^3 QED acceptance by 1.7%. Further discussion of higher order QED effects appears in Appendix II.

(b) The computation of the hadronic vacuum polarization depends on hadronic cross sections at all energies. Errors in those cross sections, particularly at low energies near resonances, lead to an uncertainty of 0.3% in our cross section. If a heavy lepton or t quark were to exist such that it could be pair produced just above currently explored

energies, near $E_{c.m.} = 46$ GeV, they would add 0.1 and 0.2% respectively. Thus the vacuum polarization terms have total uncertainty of about 0.4% in our cross section.

(c) The cross section for events with very hard initial state radiation, or low center of mass energy for the annihilation, is governed by vector meson yields near resonances which are not accounted for in the Monte Carlo. The effect on $\mathcal{A}$ from this incorrect modeling is negligible because the cross section for such events is a small fraction of the total and the detection efficiency is very small: a 10% error in the photon cross section for $k>0.7$ propagates to only a 0.25% error in $\mathcal{A}$.

(d) The s-dependence of the hadronic cross section may not scale precisely as the QED-parton level prediction of R(s)=constant between quark thresholds, even at intermediate center-of-mass energies. Indeed, the QCD factor $(1+\alpha_s(s)/\pi)$ multiplying R, ignored in the photon spectrum, does vary with $E_{c.m.}$ because the strong coupling constant runs proportional to $1/\log(s/\Lambda^2)$, but so slowly as not to change R significantly. Measurements with the TASSO[10] and JADE[13] detectors at PETRA confine possible deviations from R=constant in the range $E_{c.m.}$=12–37 GeV to about $\pm 5\%$ and hence affect $\mathcal{A}$ at the 0.4% level.

(e) Final state radiation has been explicitly ignored in the preceding analysis, because of model dependencies which should have negligible effects. Formally, radiative corrections should be applied to all charged particles involved in the fragmentation process as well as the quarks, an ill-defined calculation in perturbation theory. However, as events with and without *final state* radiative photons are not distinguished by the selection process, all final states are degenerate, and the conclusions of Lee and Nauenberg[31–32] can be applied. For such degenerate states the total radiative correction cannot contain any leading log mass singularities, *i.e.* there are no terms of order $\alpha^n\,[\log(q^2/M^2)]^m$ for positive integers n and m where $m \geq n$. Hence the correction is very small, of

order (α/π). In addition, photons may be radiated by the quarks before, along with, or after gluons. Such QED-QCD interactions have been investigated[33] and present a calculational difficulty in perturbation theory. Because of the small size of both the electromagnetic and strong coupling constants, any such effect is expected to be small.

QCD and Fragmentation

The second step in the event simulation encompasses gluon emission from the $q\bar{q}$ (γ) system and the subsequent fragmentation of quarks and gluons into hadrons. The LUND[34] Monte Carlo program has been used to perform these tasks. The Lund scheme treats the problem as three separate stochastically evolving stages, unrelated except that the output of each stage acts as input to the next: gluon emission, fragmentation into primary hadrons, and decays into final state stable particles.

Second order perturbative QCD is applied to decide if zero, one, or two gluons should be radiated, and to specify their momenta. These decisions need only two input parameters, the QCD energy scale parameter Λ=0.05–1 GeV, and a transverse mass[34] cutoff $m_t \approx 1$ GeV which defines the (arbitrary) boundaries between the three possible states. The parameter Λ sets the energy dependence of the strong coupling constant α_s, and hence of the dynamical part of the gluon emission probability. Second order QCD virtual corrections[35] have not yet been included. The quark-antiquark pair from the $q\bar{q}$ (γ) generator becomes a $q\bar{q}$, $q\bar{q}\,g$, or $q\bar{q}\,gg$ state according to the QCD cross sections parametrized in terms of $\alpha_s(s')$, where $s' = s(1-k)$. The flavor content and angular orientation are preserved in the transformation.

Two modes for fragmenting the $q\bar{q}$ $(g)(g)$ state are available in LUND, the string model[36–40] and the incoherent jet model, the latter similar to that used in the Ali[41] Monte Carlo and originally presented by Field and Feynman.[42] In the string model the

outgoing quarks and gluons stretch a "color flux bag" surrounding the interaction. The entire system is replaced formally with a relativistic, massless, color-singlet string with its diverging endpoints corresponding to the emerging quark and antiquark. Gluons are represented by points ("kinks") on the string which carry energy and momentum. The stretching string breaks in a number of places, each time producing a quark and antiquark at the freshly broken ends of string. Eventually "short" pieces of string are coalesced to form primary mesons. Primary baryons are produced by assigning a non-zero probability that a break in the string introduces a diquark-antidiquark pair at the broken ends, which later join the quark (antiquark) attached to the other end of its string fragment to form a baryon (antibaryon). Conversely, the incoherent jet model has quarks and gluons fragment essentially independently. Gluons are replaced with a quark-antiquark pair of the appropriate energies and momenta. Quarks and antiquarks are pulled out of the vacuum to produce meson states and ensure flavor, energy, and momentum conservation. In both fragmentation models there is a number of adjustable parameters which are set to give reasonable agreement between Monte Carlo predictions and experiment in a number of event properties, including exclusive and inclusive momentum spectra, multiplicity, transverse momentum spectra, and specific particle production rates.

The last stage of the Lund Monte Carlo involves the decays of primary hadrons to final state long-lived particles. Known decay modes, lifetimes, and branching ratios are implemented where measurements exist, and theoretical predictions are used elsewhere.

Detector Monte Carlo

The purpose of the detector Monte Carlo program is to accept as input an array of final state stable particle labels and momentum vectors of a hypothetical e-pair event

and produce an output event record, identical in format to real data, that simulates the response of the actual MAC detector. These event records can then be subjected to the same programs as the data to study the effects of the apparatus and analysis procedure on fundamental quantities. The primary challenge of the simulation is to reproduce realistically the characteristics of electromagnetic and hadronic cascade showers in the calorimeter, particularly on complex events such as multihadrons. Two applications-oriented computer program packages represent the state-of-the-art in this radiation transport field:[43] EGS[18] and HETC.[44] EGS deals with the interactions of electrons and photons with matter and HETC with hadrons and muons. The combined use of these programs forms the core of the detector Monte Carlo.

The actual geometry and materials characteristic of the MAC detector have been coded for use by EGS and HETC, including the aluminum vacuum pipe, central drift chamber aluminum walls and steel endplates, aluminum solenoid coil, central shower chamber aluminum extrusions and lead-alloy absorber layers, central and endcap calorimeter iron plates, endcap chamber frames, and the gas mixture inside the proportional chambers. The pulse heights from the PWC's are scaled from actual energy deposition in the gas to simulated digitized counts by an empirically determined calibration factor. Charged pions, protons, neutrons, and muons are transported by HETC; electrons, positrons, and photons, including those resulting from π^0 and μ decay, are handled by EGS. For the purposes of energy deposition, a few hadrons unknown to HETC must be replaced by familiar particles of the same momentum in the central drift chamber and same kinetic energy in the calorimeter: $K^{\pm} \rightarrow \pi^{\pm}$, $K^0_L \rightarrow n$, $\bar{p} \rightarrow \pi^-$, and $\bar{n} \rightarrow n$. The $K^{\pm}$ identity is retained, however, for its weak decay, though the only mode presently allowed is $K \rightarrow \mu\nu$.

The detector Monte Carlo also incorporates detailed simulations of the hardware and software trigger systems, central drift chamber, toroid spectrometer, and outer muon drift chambers. It models the actual geometry and response of the 144 scintillation counters, the thresholds and logic for all triggers, the bending of charged particle trajectories inside the magnetic fields of the solenoid and toroid coils, individual cell efficiencies and time resolution in the inner and outer drift systems, and extra central drift "noise" hits caused in the real chamber by electronic cross-talk, ultra-violet photon conversions, and knock-on electrons.

Appendix II Higher Order Radiative Corrections

The electromagnetic cross sections (Bhabha scattering, and μ-pair production) needed for the determination of luminosity were computed by means of the Berends, Kleiss, and Jadach programs[45]. This calculation generates events according to a computation exact through α^3. Potentially, there are substantial uncertainties in this calculation due to higher order effects when one attempts to measure cross sections to an accuracy of a few percent. For example, the lowest order correction for vacuum polarization is about 10%; therefore one expects an error of the order of the square, 1%, from this source alone. Similarly, the vertex corrections for the initial and final state are each about 7%, so two additional errors of the order of 0.5% are expected. A cut on the acollinearity angle is potentially troublesome due to the emission of multiple photons; for tight cuts large discrepancies in the distribution of the acollinearity angle are observed unless one adopts exponentiation of the bremsstrahlung part of the correction. For the cuts made in this experiment these errors are estimated to be 3 to 4%. This kind of analysis indicates that the α^3 cross section could have systematic errors for electromagnetic cross sections of the order of 5%. The production of hadrons proceeds much like the μ-pairs except that there is no acollinearity cut and final state radiation effects may be neglected (*cf.* subsequent discussion). As a result the systematic error for hadron production due to higher order QED effects is smaller, of the order of 2%. As will be discussed, comparison with more quantitative estimates of higher effects indicates that in fact there is a large cancellation of the potential errors, and the lowest order result differs from the higher order result by $\leq 2\%$. This high degree of cancellation is unexpected.

Y.S. Tsai[46] has used the renormalization group equations to estimate the radiative corrections summing all leading logs, *i.e.* summing all contributions of the form $(\alpha \log q^2)^n$. The result is remarkably simple. Let the α^3 cross section be written

$$d\sigma_3 = d\sigma_2(1 + 2\Re\Pi + \delta_r) ,$$

where $d\sigma_2$ is the lowest order (α^2) cross section, $\Re\Pi$ is the real part of the vacuum polarization,

$$\Pi(s) = \frac{-\alpha s}{3\pi} P \int_0^\infty \frac{R_t(s')}{s'(s'-s)} ds' - \frac{i\alpha}{3} R_t(s) ,$$

and δ_r is the remaining radiative correction. The quantity R_t is the ratio of the total cross section for e^+e^- annihilation, including leptons, to the μ-pair production cross section. (Note, the contribution to R_t for electrons is 1.) P denotes a ***principal value***, and s denotes the square of the center of mass energy. Tsai's result is

$$d\sigma_\infty = d\sigma_2 \frac{1}{|1-\Pi|^2} (1 - \Re\Pi)^{-\delta_r/\Re\Pi} .$$

By construction this expression reverts to the α^3 expression when expanded in α; furthermore it is similar to exponentiated behavior in the limit of small photon energies. The factor $1/|1-\Pi|^2$ represents the sum of all bubble diagrams in the vacuum polarization modification of the propagator.

There are experimental uncertainties in the input to the vacuum polarization correction. These are due partly to uncertainties in the hadron production cross section at energies other than those measured and partly due to unknown physics. The primary uncertainty due to imprecise hadron cross sections comes from low energy cross sections, below 3 GeV center of mass energy. These uncertainties lead to uncertainties in the cross sections of 0.0, 0.2, 0.3, and 0.3 % for the luminosity monitor, large angle

Bhabha scattering, μ-pair, and hadron production respectively. In addition physics at energies above those presently explored can have an effect. For example heavy lepton pair production at 46 GeV, just above the presently explored limits, would change the cross sections by 0.0, 0.0, 0.1, and 0.1 %. Similarly if the quark flavor *top* had a threshold of 46 GeV it would induce changes in our cross sections of 0.0, 0.0, 0.2, and 0.2 %-respectively. As a result we assign uncertainties of 0.1, 0.3, 0.4, and 0.4 % due to vacuum polarization corrections to our cross sections for the luminosity monitor, large angle Bhabha scattering, μ-pair, and hadron production.

For hadron production the effects of final state radiation have been neglected, by virtue of the Lee and Nauenberg theorem,[31–32] which says that there are no leading logs for final state radiation when one sums over all degenerate final states. This means that the correction for the final state is just $1 + \alpha/\pi$, to lowest order in α. This correction is 0.23%, and has been ignored. (It is not clear whether this correction applies to the entire final state or whether it depends upon the number of possibly radiating hadrons. As a result we assign an uncertainty of 1%.)

Detailed comparisons have been made between the α^3 calculation and Tsai's calculation for Bhabha scattering, μ-pair production, and hadron production for the selection criteria employed in this experiment. The differences were never more than 2%.

While Tsai's treatment sums all leading logs, there is a problem of principle in its handling of hard photon emission by the initial e^+e^- system. For hard photons the remaining center of mass energy for the annihilation will be much lower than the original energy, resulting in a kinematic enhancement of the cross section. This enhancement is further increased by the higher order correction formalism, and the justification for this is unclear. Quantitatively, however, the uncertainty introduced by this effect for this experiment is $\approx 0.3\%$. Another problem of principle is that the formulation does not

properly treat the effect of multiple photon emission on the acollinearity distribution for electromagnetic cross sections. Tsai's result really describes the total energy radiated in the form of photons, but it does not treat the momentum. A simple calculation was made to estimate the effect of this error: Each initial state lepton was allowed to radiate in a Weizacker-Williams approximation and the distribution of net photon momentum computed compared to the same calculation if only one lepton or the other radiated. For the luminosity monitor the Tsai acceptance should be increased by 0.2%, for central Bhabha scattering, 0.4%, and for μ-pairs, 0.6%. Our results employing the higher order terms have applied these corrections. Finally, one must consider the effect of non-leading log terms in the treatment, *i.e.* terms of the form $\alpha^m \log^n q^2$, where $m > n$. (The case $m < n$ cannot occur.) These were estimated by examining Tsai's fourth order terms in α and dividing them by $\log q^2/m^2$, where m is the mass appropriate to the process. The resulting uncertainties are of the order 0.2% for the QED processes and perhaps as much as 1.0% for hadron production.

Numerical problems were encountered in computing the small angle Bhabha scattering cross section with radiative corrections. Three different programs[47,19] were used for this purpose giving slightly different results for the final cross section. From the spread of these results we have assigned an error of 1.5% to radiative corrections for the luminosity monitor.

Unfortunately Tsai's formalism is not applicable to the $\gamma - \gamma$ final state. We have applied the same correction for collinearity for this process as for Bhabha scattering, since the same initial state radiation considerations apply. No other higher order corrections have been applied. Note that there is no vacuum polarization correction to order α^3 for this process, so that there is less sensitivity to this type of correction. The lesson of the other QED cases is that the lowest order result does rather well, so that we

have chosen not to tamper with it further. We assign a 1% uncertainty to the radiative corrections for this process.

Table 24 summarizes the magnitude of the corrections and their uncertainties applied over and above the α^3 calculation. A negative number means that the corrected cross section using the higher order calculation is smaller than the cross section corrected only through α^3. (The acollinearity entry refers to a correction to the Tsai result.)

Table 24

Higher Order Corrections and Their Uncertainties in %.

Correction	Luminosity Monitor	Bhabha Scattering	Photon pairs	μ pairs	Hadrons
Leading log	–0.3	–0.2	–	–0.1	–1.7
Acollinearity cut	–0.2	–0.4	–0.4	–0.6	
Total	–0.5	–0.6	–0.4	–0.7	–1.7
Uncertainty	0.2	0.4	1.0	0.4	1.0

As an example of application of this table, assume that only large angle Bhabha scattering is used for the luminosity measurement. The resulting hadron cross section, effectively the ratio of the corrected hadron yield to Bhabha scattering yield, corrected for higher order effects is $(1.7 - 0.6) = 1.1\%$ smaller than that obtained when only α^3 radiative corrections have been computed.

Appendix III Two Photon Background

We have calculated the two-photon background by Monte Carlo methods; it consists of two parts. Because of the MAC acceptance the larger is from "hard scattering" of quarks[48] and the other is from a Vector meson Dominance Model.[49] In both cases the events from the physical process were generated and the resulting particles followed into the MAC detector in the same manner as the one-photon annihilation events.

Hard Scattering

For moderately large momentum transfers to the electron (positron), which characteristically happens for two-photon events passing the one-photon acceptance criteria, the dominant contribution to the two-photon background is the quark pair production mechanism analogous to the QED reaction, $e^+e^- \rightarrow e^+e^-\mu^+\mu^-$. The program of Vermaseren *et al.*[48] has been used to generate quark-antiquark pairs in which at least one quark had an angle $|\cos\theta| < 0.98$ and the total energy of the quark pair is at least 4 GeV. The quark pairs were then allowed to fragment using the Monte Carlo program of Ali *et al.*[41] Because of the small center of mass energy involved, the gluon emission was ignored. The charm contribution has been computed using a recently measured fragmentation function.[50] No radiative corrections have been included on this process. The same detector Monte Carlo simulation was used on the resulting events as for the one-photon annihilation simulation to determine the cross section accepted by our selection criteria. It is assumed that no events in the excluded region of phase space would have been accepted.

Vector Dominance Model

The total multi-hadron production cross section due to photon-photon collisions has

been measured by the PLUTO[24] and TASSO experiments[51,25] at PETRA. The results are reasonably well described by the VDM hypothesis which assumes that the photons interact via vector mesons, predominantly ρ mesons, which in turn scatter like hadrons. The total photon-photon multi-hadron production cross section is predicted to be[49]

$$\sigma_{\gamma\gamma} = \left[240 + \frac{270}{E_{c.m.}\ (GeV)}\right]\ (nb)\ ,$$

where $E_{c.m.}$ is the center of mass energy of the hadronic system. Within the quoted errors the PLUTO and TASSO measurements are roughly consistent with this prediction for $E_{c.m.} > 1$ GeV, however the TASSO cross section is about 50% larger than the PLUTO cross section. We have used a Monte Carlo program written by L. Golding and D. Burke,[53] which uses the predicted cross section. The cross section for $e^+e^- \rightarrow e^+e^- + hadrons$ is then given by the convolution of this cross section with the photon flux factor as given by the Weizaker-Williams approximation,

$$\frac{d\sigma}{dk} = \frac{\alpha}{\pi k}[1 + (1-k)^2] \log\frac{E_b}{m_e}\ ,$$

where k is the energy of the photon in units of the beam energy. Multi-hadron events are generated assuming an all-pion model. For a given center of mass energy for the hadronic system, $E_{c.m.}$, the charged multiplicity is given by

$$N_{ch} = 2.1 + 1.6\ \log E_{c.m.}\ (GeV)$$

in accordance with one-photon annihilation measurements at lower center-of-mass energies. The hadrons are assumed to have limited transverse momentum with respect to the $\gamma - \gamma$ axis with a Gaussian distribution having a standard deviation of 0.5 GeV. The fraction of charged to neutral pions was fixed at 2:1, also suggested by measurements.

The PLUTO experiment[24] observed that the photon-photon cross section is suppressed by the form factor of the ρ meson as given by

$$F(q^2) = \frac{1}{1 - q^2/m_\rho^2}$$

as the q^2 of one of the electrons becomes large; m_ρ is the mass of the ρ meson. This corresponds to the case where one of the electrons is scattered by a non-zero angle; this factor was included in our calculation.

Cross Check with Data

Cross checks on the two-photon background contributions have been made using the actual data. Single-tagged events are expected to be almost exclusively due to hard scattering two-photon events, because of the large momentum transfers involved; this is confirmed by the above calculations. We found that a sample of single-tagged events is well described by the hard scattering alone, so we believe that this component is well represented by the calculation. We have selected single-tagged events with an electron (positron) having an angle $\theta > 18°$ and an energy of at least 6 GeV. After correcting for acceptance and detection efficiency the number of background subtracted events is in good agreement with the prediction of hard scattering model described above; the VDM model predicts a negligible yield for such events. Details of this work will be given in another publication.

As described in the main text we have also used a control sample of the data near the one-photon sample; this control sample is more sensitive to the VDM contribution than the hard scattering contribution. This sample indicates that the VDM calculation above is somewhat too low. If instead one used the cross section measured by TASSO the agreement would be better; accordingly, we have multiplied the VDM calculation by

a factor of 1.5. In view of the discrepancy between the PLUTO and TASSO data, and the fact that the results are expected to be sensitive to some of the input parameters, we have assigned a 50% error to this background calculation.

References

(a) Present address: Cyclotron Laboratory, Harvard University, Cambridge, MA 02138.

(b) Present address: CERN, Geneva, Switzerland.

(c) Present address: Los Alamos National Laboratory.

(d) Present address: Lawrence Berkeley Laboratory.

(e) Present address: Mechanical Engineering Department, Stanford University, Stanford CA 94305.

(f) Present address: Metaphor Computer Systems, 2500 Garcia Ave., Mountain View CA 94043.

(g) Present address: Chungnam National University, Dept. of Physics, Daejon, 300-31, Korea.

(h) Present address: Laboratory of Nuclear Studies, Cornell University, Ithaca NY 14853.

1. M. Dine and J. Sapirstein, Phys. Rev. **43**, 668 (1978).
2. V.G. Chetyrkin, A.L. Kataev, and F.V. Tkachev, Phys. Lett. **85B**, 277 (1978).
3. W. Celmaster and R.J. Gonsalves, Phys. Rev. Lett. **44**, 560 (1979).
4. G. Wolf, XIV International Symposium on Multiparticle Dynamics, Granlibakken, Lake Tahoe, U.S.A. 1983.
5. T. Bolongnese *et al.*, Phys. Rev. Lett. **50**, 224 (1983).
6. D. Bollini *et al.*, Physics Letters **107B**, 403 (1981).
7. C. Klopfenstein *et al.*, CUSB 83-07 (1983).
8. P. Avery *et al.*, CLNS 83-582 (1983).

9. TASSO Collaboration, DESY 84-57 (1984), submitted to Z. Phys. C.

10. R. Brandelik *et al.*, Phys. Lett. **113 B**, 499 (1982).

11. J. Burger *et al.*, Proc 21^{st} Int. Conf. on High Energy Physics, Paris (26-31 July 1982).

12. R. Hollebeek *et al.*, Proc 21^{st} Int. Conf. on High Energy Physics, Paris (26-31 July 1982).

13. W. Bartel *et al.*, Phys. Lett. **129B**, 145 (1983)

14. MAC Collaboration, Proc. Int. Conf. on Instrumentation for Colliding Beams, ed. W. Ash, SLAC-Report 250 p. 174.

15. G. Gidal, B. Armstrong, and A. Rittenberg, LBL Report LBL-91 (1983).

16. R.L. Anderson *et al.*, IEEE Trans. Nucl. Sci. **NS-25**, 340 (1978).

17. B.K. Heltsley, University of Wisconsin-Madison PhD. Thesis, WISC-EX-83/233, July 1983.

18. R.L. Ford and W.R. Nelson, SLAC Report 210 (1978).

19. F.A. Berends and R. Kleiss, Nucl. Phys. **B228**, 537 (1983). Two different versions of this program were tested.

20. M.C. Delfino, University of Wisconsin-Madison PhD. Thesis, in preparation.

21. F.A. Berends and R. Kleiss, Nucl. Phys. **B186**, 22 (1981).

22. F.A. Berends and R. Kleiss, Nucl. Phys. **B177**, 237 (1981).

23. E. Fernandez, *et al.*, Phys. Rev. Lett. **50**, 1238 (1983).

24. PLUTO collaboration, Phys. Lett. **89B**, 120, (1979).

25. N. Wermes, PhD. Thesis, Bonn University, report BONN-IR-82-27 (1982).

26. This value is about half the value given in the 1982 Particle Data Book, but agrees with the current measurements; *cf.* MAC Collaboration, Proceedings of

the International Conference on High Energy Physics, Paris (1982), p. C3-52, Mark-II Collaboration, Phys. Rev. Lett. **49**, 1369 (1982), CELLO Collaboration, Phys. Lett. **114B**, 282 (1982), TPC Collaboration, LBL180014 (June 1984).

27. S. Clearwater, Stanford University PhD. Thesis, SLAC Report 264, November 1983.
28. C. Peterson *et al.,* Phys. Rev. **D27**, 105 (1983).
29. S.D. Drell, Proc. 1981 International Symposium on Lepton and Photon Interactions at High Energy, Bonn, p. 1005.
30. M. Davier, Proc. SLAC Summer Institute on Particle Physics (July 1984), reviews the situation.
31. T.D. Lee and M. Nauenberg, Phys. Rev. **133**, 1549 (1964).
32. T. Kinoshita, J. Math. Phys. **3**, 650 (1962).
33. E. Laerman, *et al.,* Nucl. Phys. **B207**, 205 (1982).
34. T. Sjöstrand, University of Lund Reports LU TP 82-3 and 82-7, (1980).
35. R.K. Ellis, D.A. Ross, and A.E. Terrano, Nucl. Phys. **B178**, 421 (1981).
36. B. Andersson, G. Gustafson, and C. Peterson, Nucl. Phys. **B135**, 273 (1978); and Zeit. Physik **C1**, 105 (1979).
37. B. Andersson and G. Gustafson, Zeit. Phys. **C3**, 223 (1980).
38. B. Andersson, G. Gustafson, and T. Sjöstrand, Zeit. Phys. **C6**, 235 (1980); Phys. Lett. **94B**, 211 (1980), and Nucl. Phys. **B197**, 45 (1982).
39. B. Andersson, G. Gustafson, I. Holgersson, and O. Månsson, Nucl. Phys. **B178**,242 (1981).
40. B. Andersson, G. Gustafson, G. Ingleman, and T. Sjöstrand, Zeit. Phys. **C13**, 361 (1982).

41. A. Ali, E. Pietarinen, and J. Willrodt, DESY T-80/01 (1980); A. Ali, E. Pietarinen, G. Kramer, and J. Willrodt, Phys. Lett. **93B**, 155 (1980).

42. R.D. Field and R.P. Feynman, Phys. Rev. **D 15**, 2590 (1977) and Nucl. Phys. **B136**, 1 (1978).

43. An excellent review of this field with details of such programs is contained in *Computer Techniques in Radiation Transport and Dosimetry*, edited by W.R. Nelson and T.M. Jenkins, Plenum Press, New York (1980).

44. T.A. Gabriel and B.L. Bishop, Nucl. Instr. Meth. **155**, 81 (1978).

45. F.A. Berends, R. Kleiss, and S. Jadach, Nucl. Phys. **B202**, 63 (1982).

46. Y.S. Tsai, SLAC PUB 3129 (1983).

47. F.A. Berends, R. Gastmans, and K.J.F. Gaemers, Nucl. Phys. **B68**, 541 (1974).

48. R. Bhattacharya, J. Smith, and G. Grammer, Jr., Phys. Rev. D **15**, 3267 (1977), and J. Smith, J.A.M. Vermaseren, and G. Grammer, *loc. cit.* p. 3280.

49. S. J. Brodsky. J. Physique, **C-2**, Suppl. **3**, 69 (1974).

50. E. Fernandez *et al.,* Phys. Rev. Lett. **50**, 2054 (1983).

51. E. Hilger, DESY 80-75 (1980).

52. N. Wermes, PhD. Thesis, Bonn University, report BONN-IR-82-27 (1982).

53. We wish to thank D. Burke and L. Golding for making their program available to us.

Figure Captions

1. Cross section views of MAC detector, (a) end view fo central section; (b) side view. Key to symbols, CD: central drift chamber, SC: shower chamber, TC: timing scintillator, HC: hadron calorimeter, EC: endcap calorimeter, MI and MO: inner and outer muon chambers.
2. Efficiency for Monte Carlo hadronic events passing the selection criteria as a function of (a) the radiative photon energy, k, in units of the beam energy, and (b) the direction of the thrust axis $|\cos\theta_T|$.
3. Comparison of data (points) and Monte Carlo calculations (histogram) for distributions of (a) E_v, (b) E_t, (c) I, (d) N_{ch}, (e) P, and (f) $\cos\theta_T$.
4. Distribution of N_{ch} for data (solid line) and Monte Carlo (dashed line) before (a) and after (b) the scaling of the Monte Carlo distribution. Event selection required $N_{ch} \geq 5$, $E_v > 16$ GeV, and $\cos\theta_T^p \leq 0.57$.
5. Distribution of E_v for data (solid line) and Monte Carlo (dashed line). Event selection required $N_{ch} \geq 9$, and $\cos\theta_T^p \leq 0.57$.
6. Distribution of E_v for data (solid line), one-photon Monte Carlo (dashed line), and two-photon Monte Carlo (dotted line).
7. Feynman diagrams included in the computation of the cross section for $e^+e^- \rightarrow q\bar{q}\ (\gamma)$.

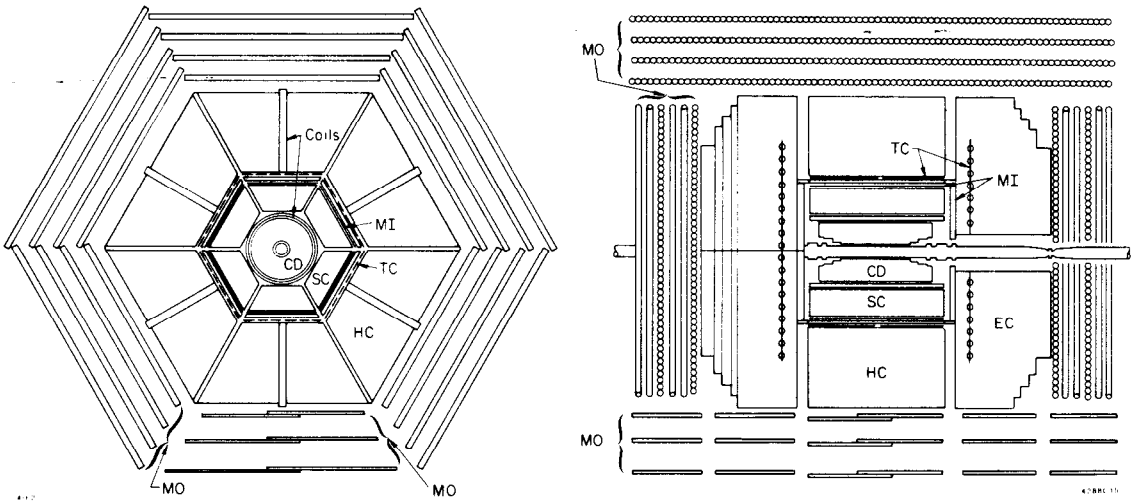

Fig. 1

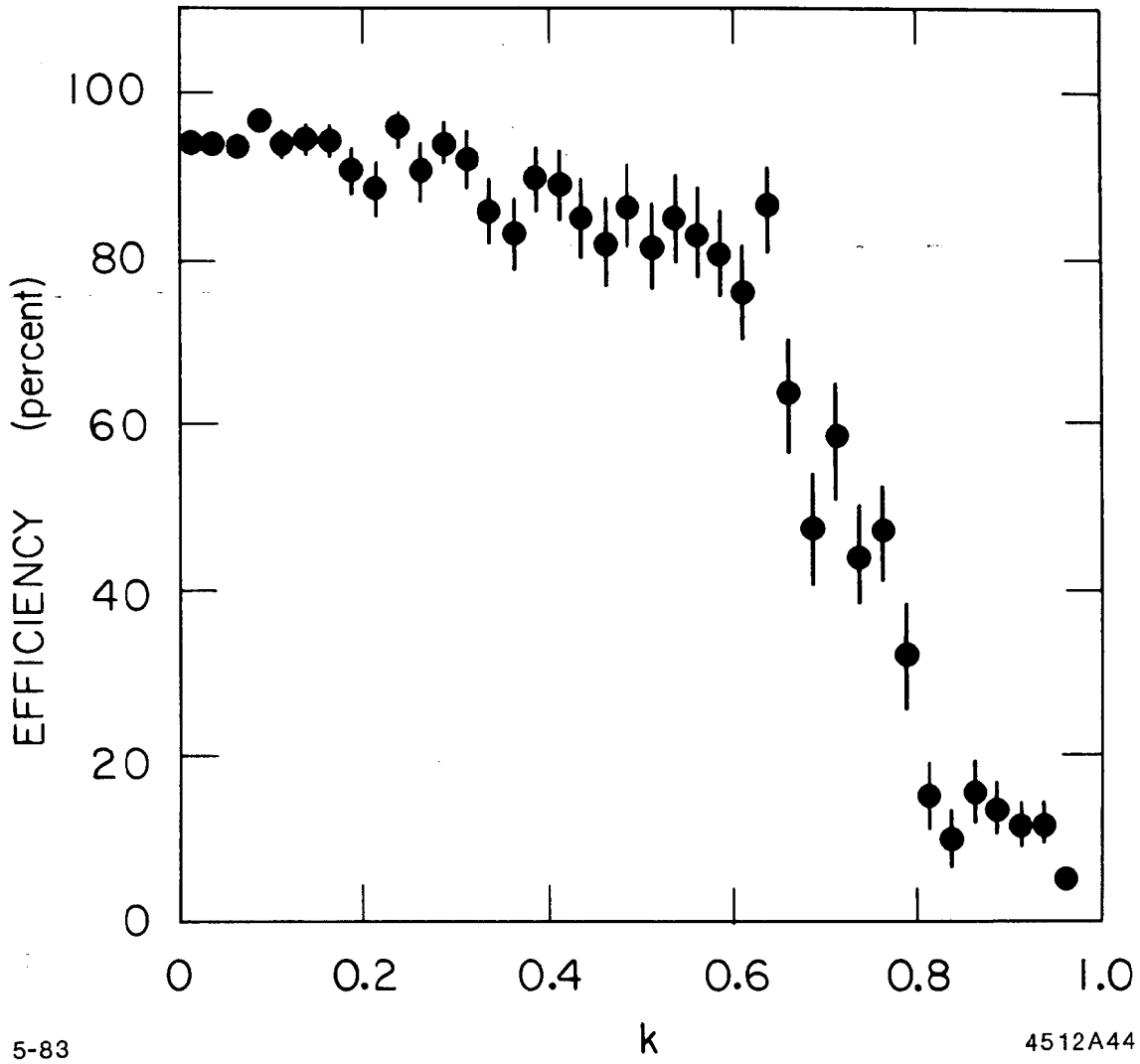
100
80
60
40
20
0
EFFICIENCY (percent)
0
0.2
0.4
0.6
0.8
1.0
k
5-83
4512A44

Fig. 2A

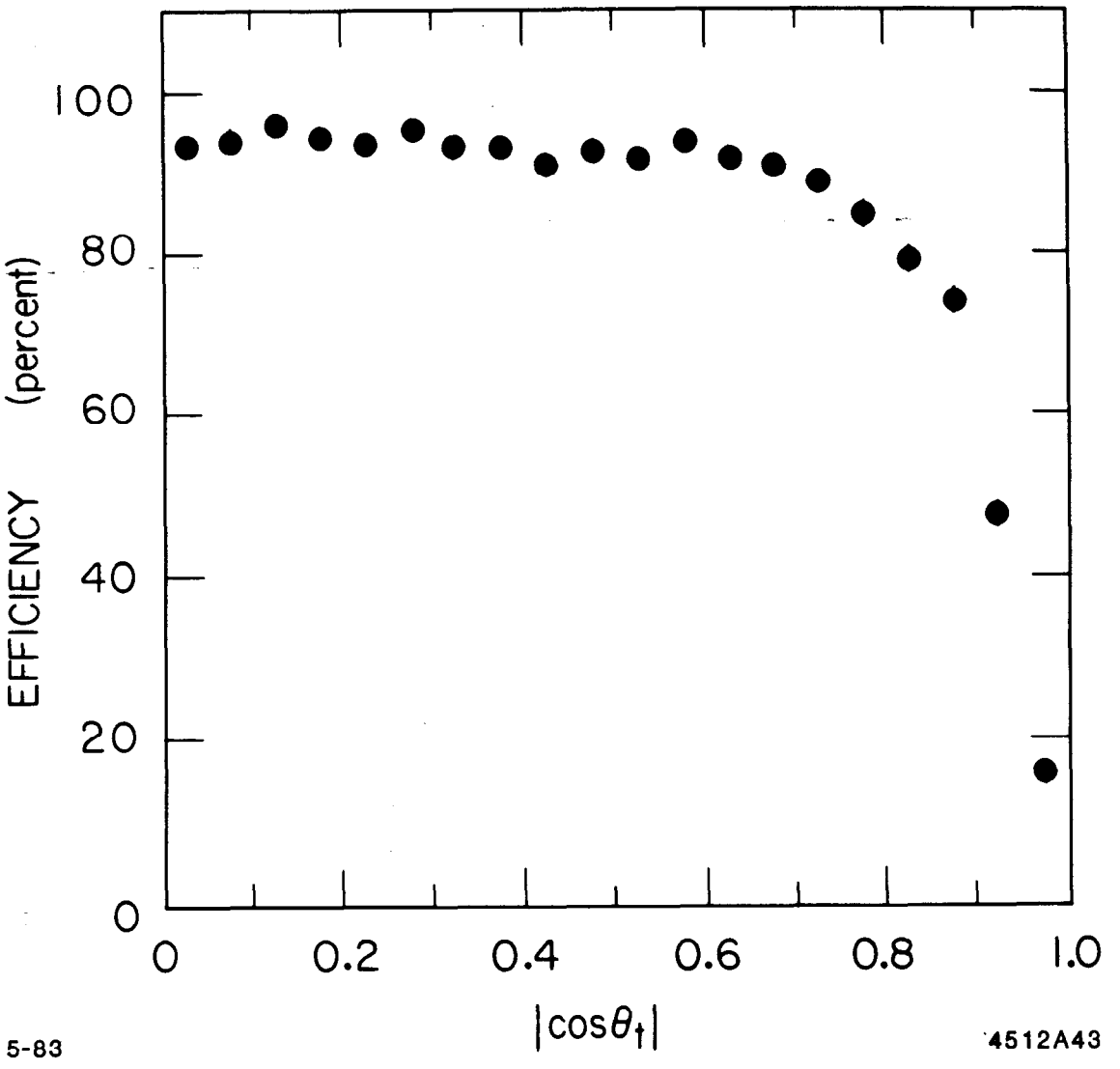
100
80
60
40
20
0
EFFICIENCY (percent)
0
0.2
0.4
0.6
0.8
1.0
|cosθt|
5-83
4512A43

Fig. 2B

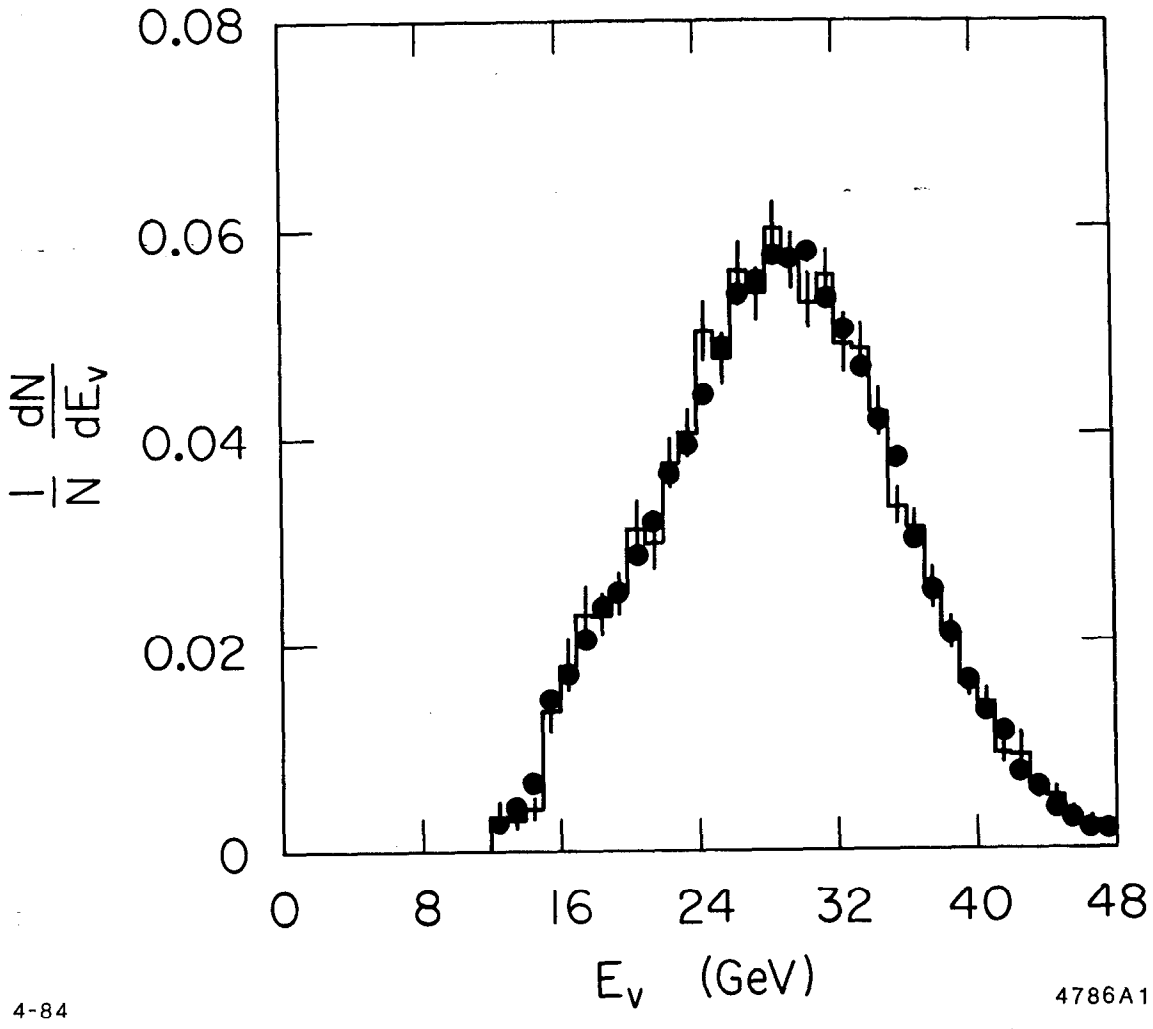
0.08
0.06
0.04
0.02
0
0
8
16
24
32
40
48
$\frac{1}{N}\frac{dN}{dE_\nu}$
E_ν (GeV)
4-84
4786A1

Fig. 3A

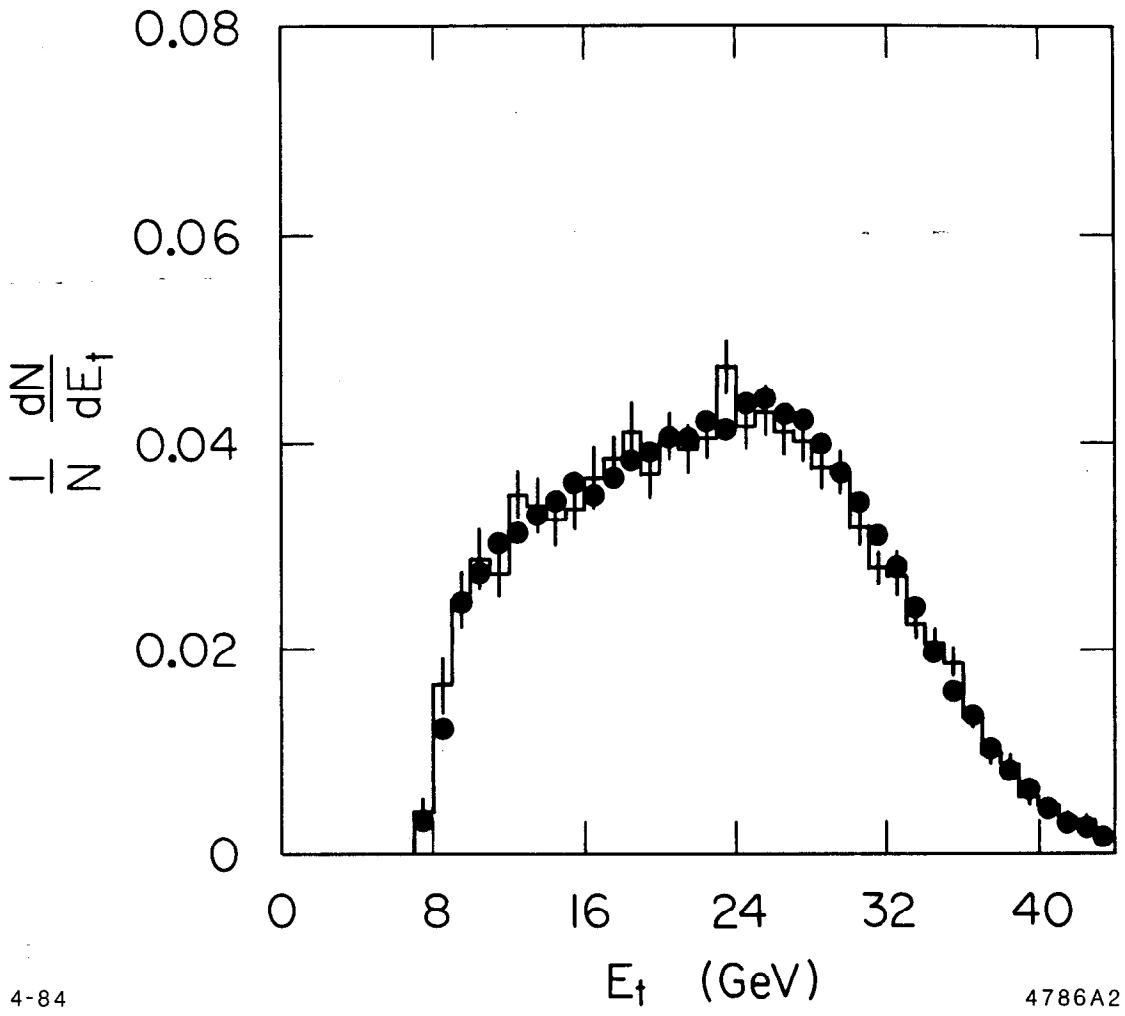
0.08
0.06
0.04
0.02
0
$\frac{1}{N}\frac{dN}{dE_t}$
0
8
16
24
32
40
E_t (GeV)
4-84
4786A2

Fig. 3B

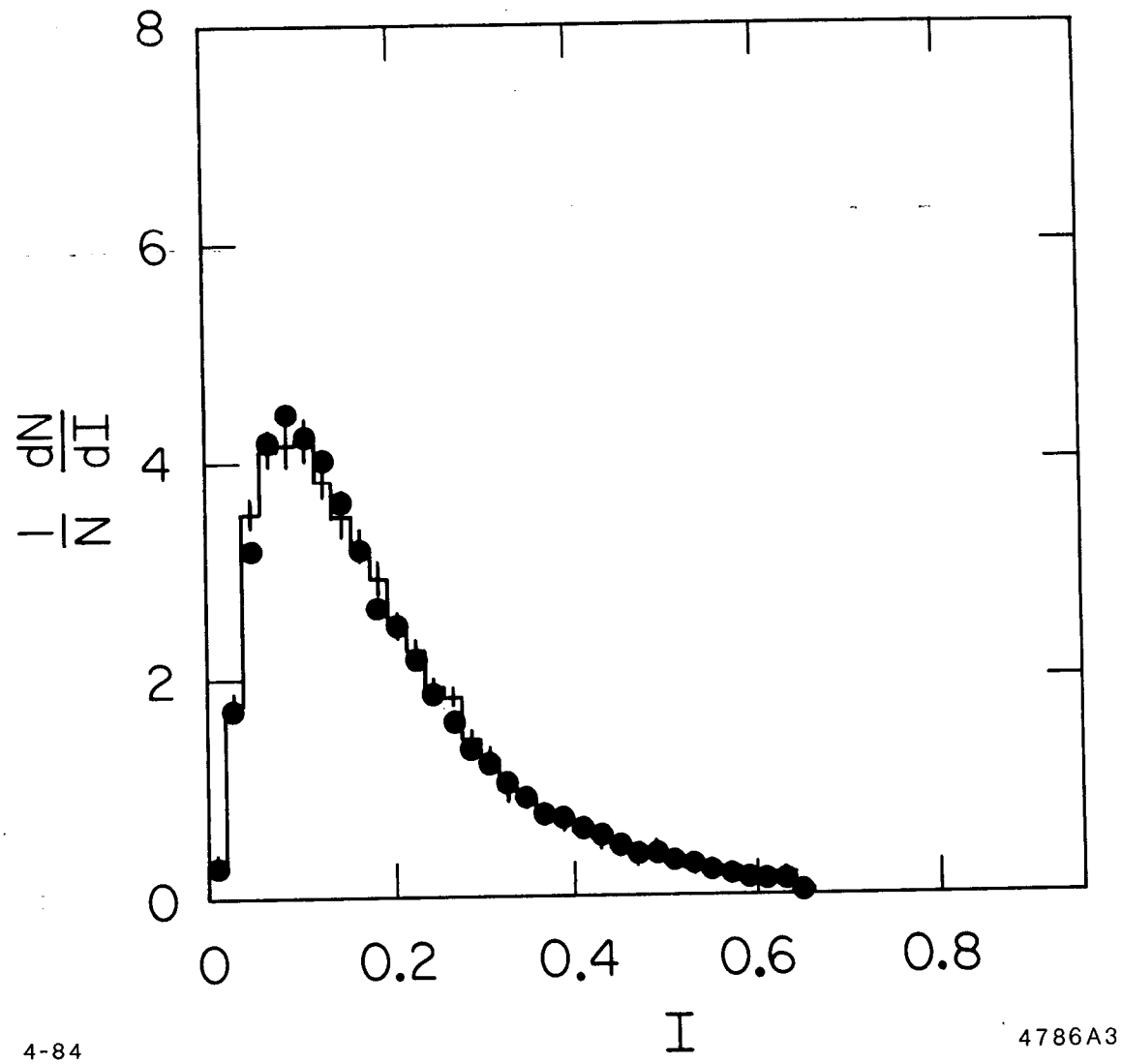

Fig. 3C

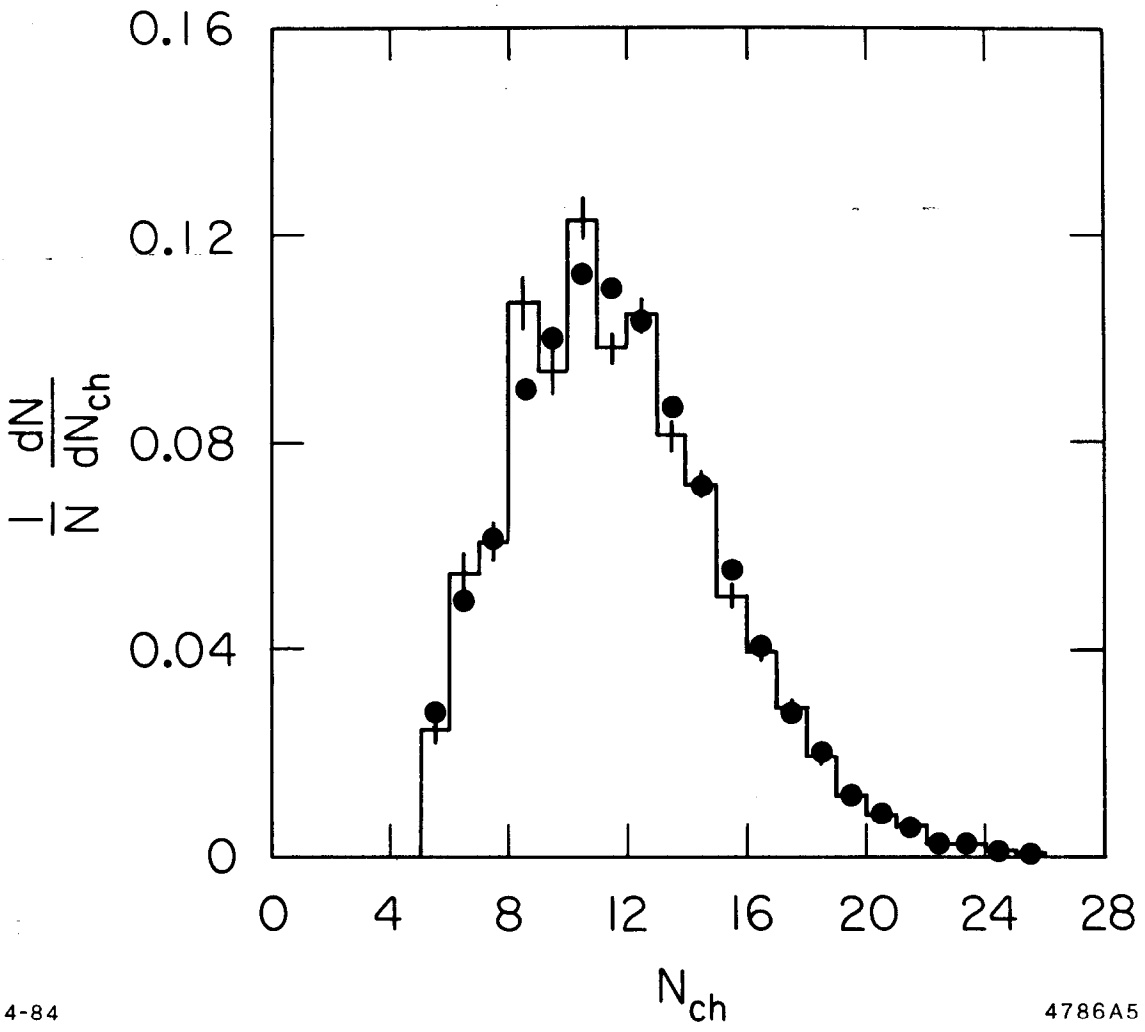
0.16
0.12
0.08
0.04
0
$\frac{1}{N}\frac{dN}{dN_{ch}}$
0
4
8
12
16
20
24
28
N_{ch}
4-84
4786A5

Fig. 3D

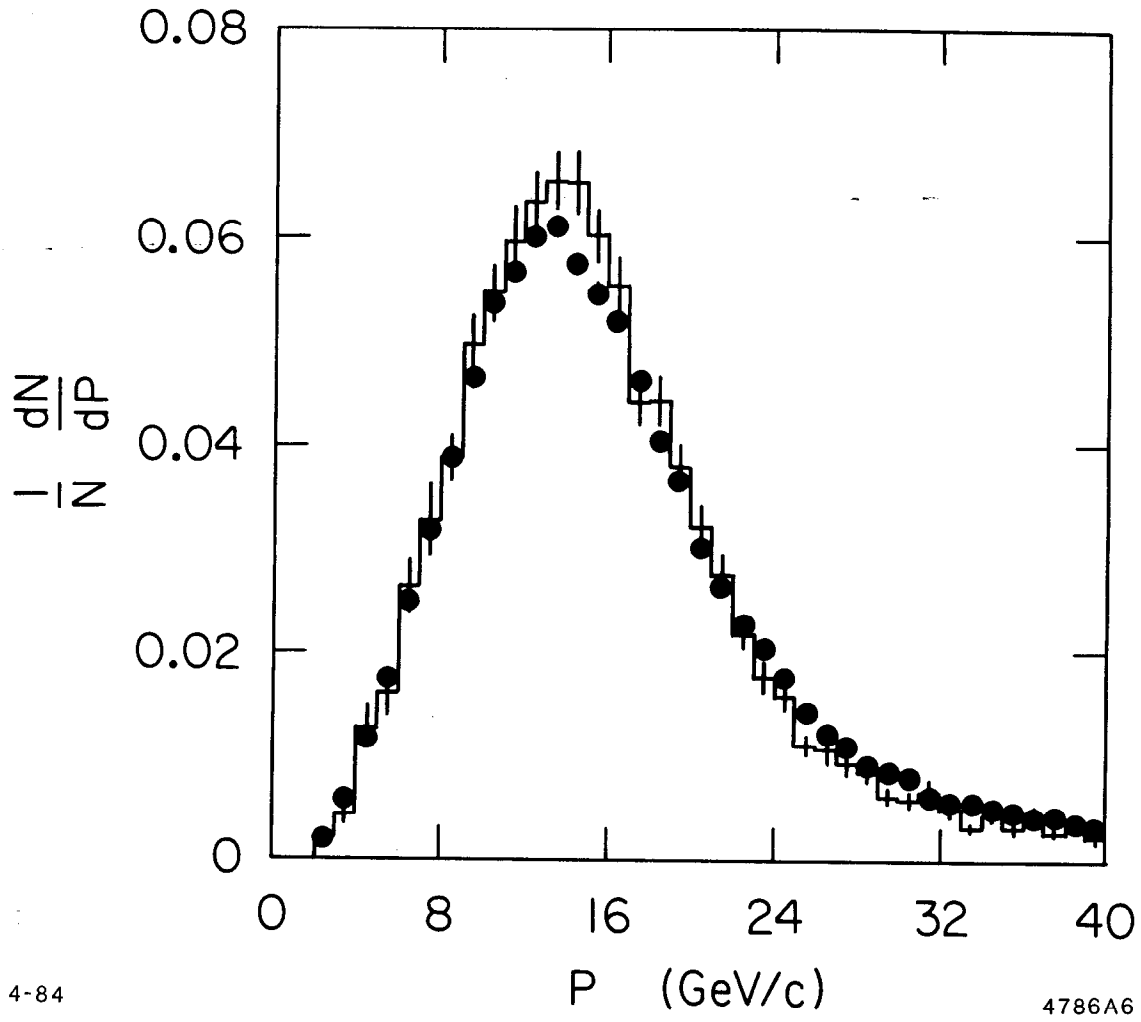

Fig. 3E

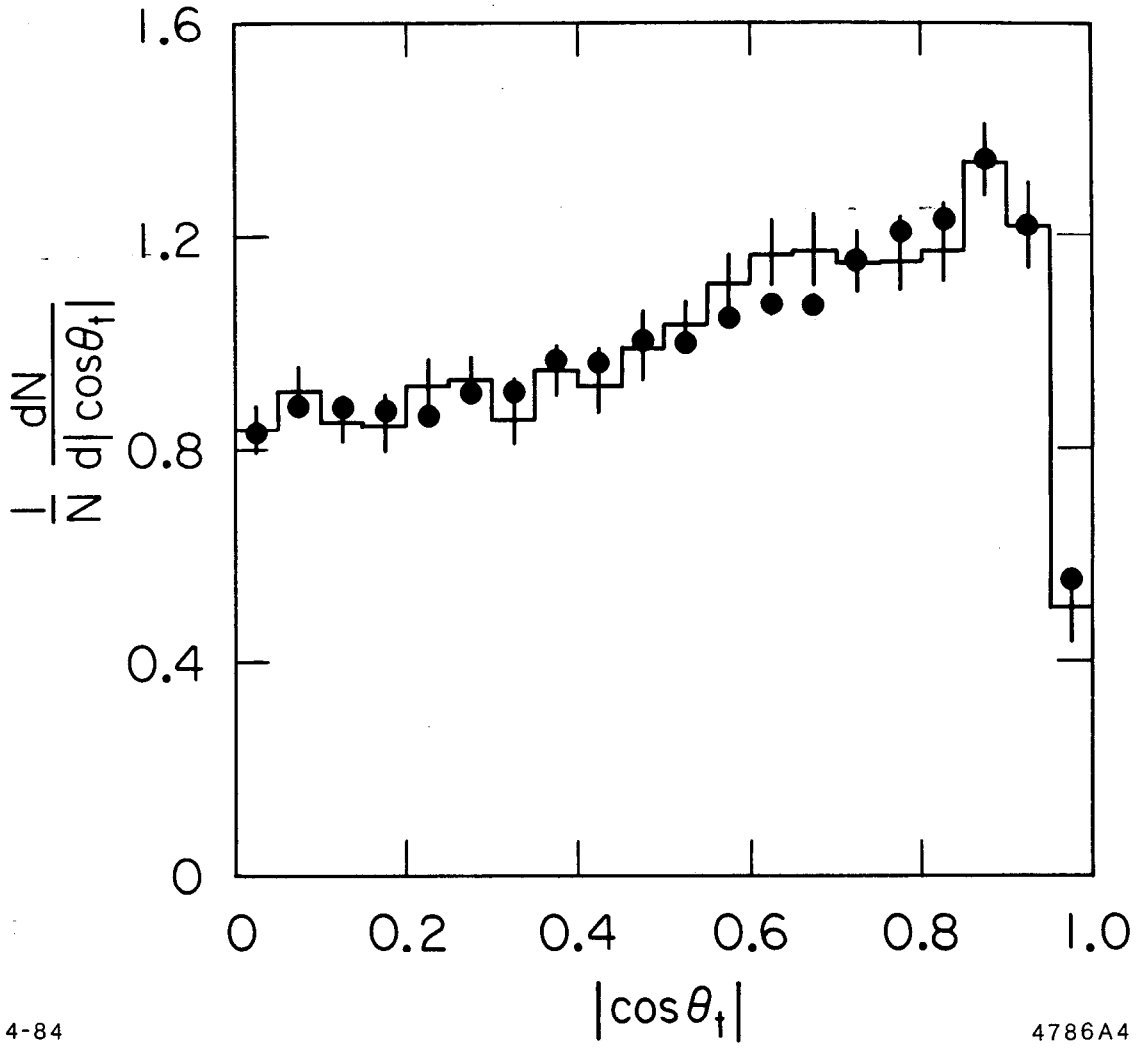
1.6
1.2
0.8
0.4
0
0
0.2
0.4
0.6
0.8
1.0
$\frac{1}{N}\frac{dN}{d|\cos\theta_t|}$
$|\cos\theta_t|$
4-84
4786A4

Fig. 3F

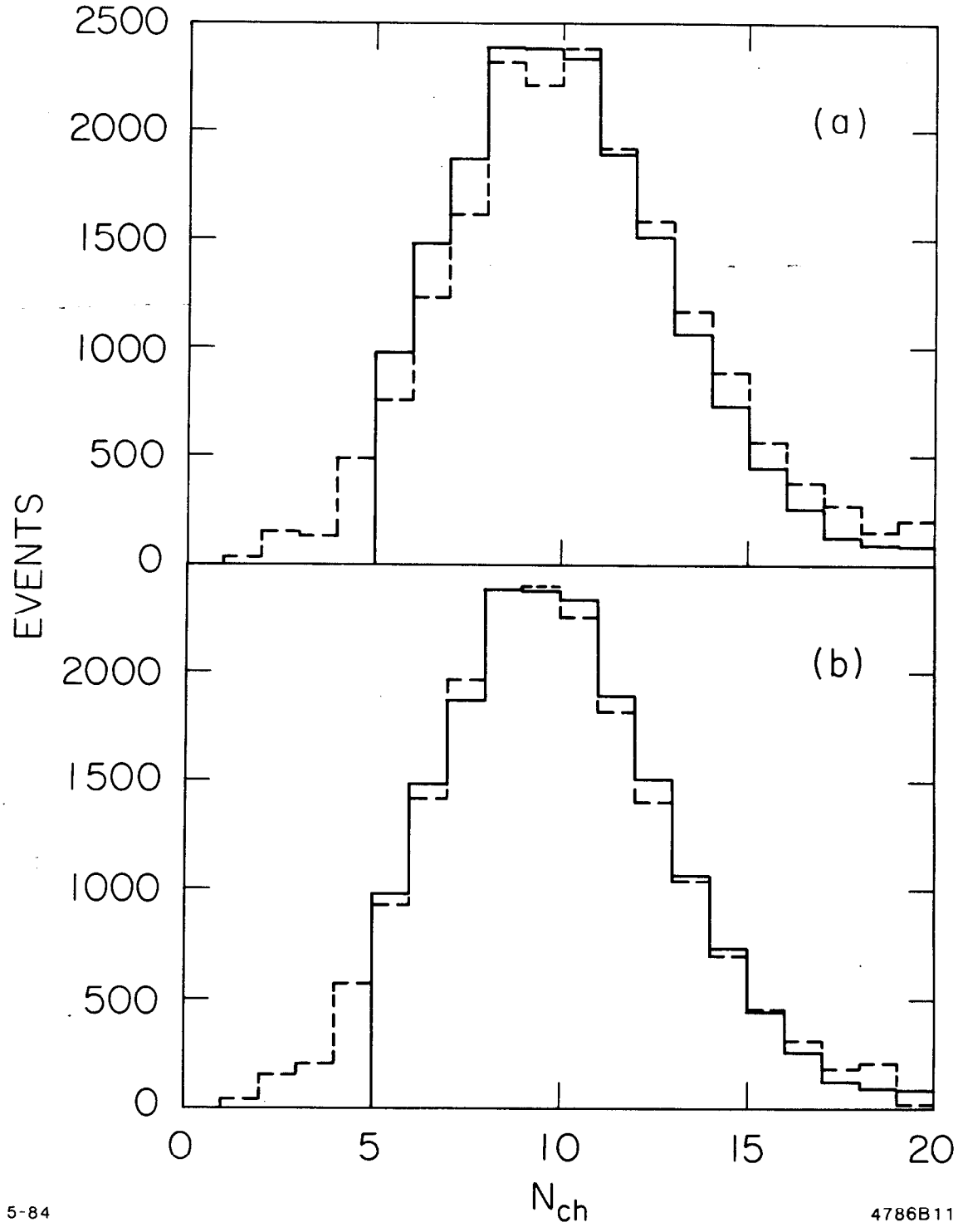
2500
2000
1500
1000
500
0
EVENTS
(a)
2000
1500
1000
500
0
(b)
0
5
10
15
20
N_{ch}
5-84
4786B11

Fig. 4

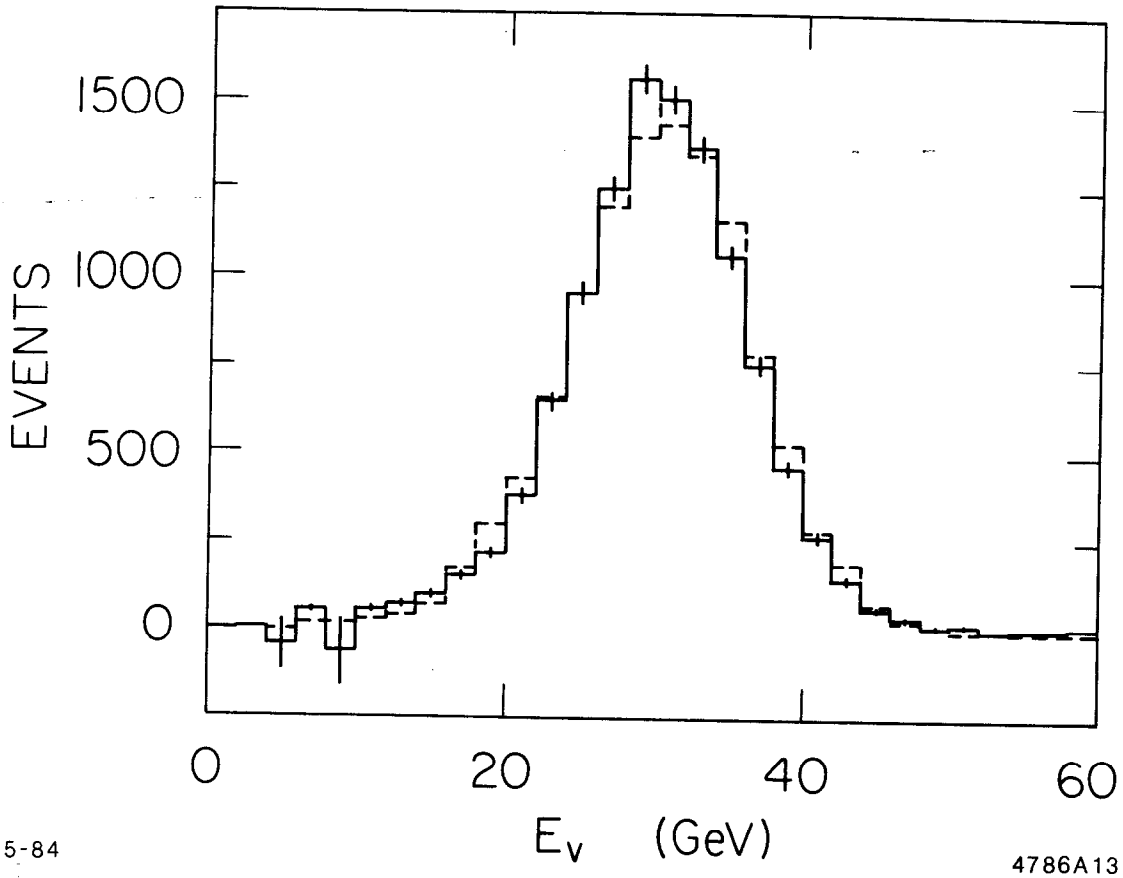

Fig. 5

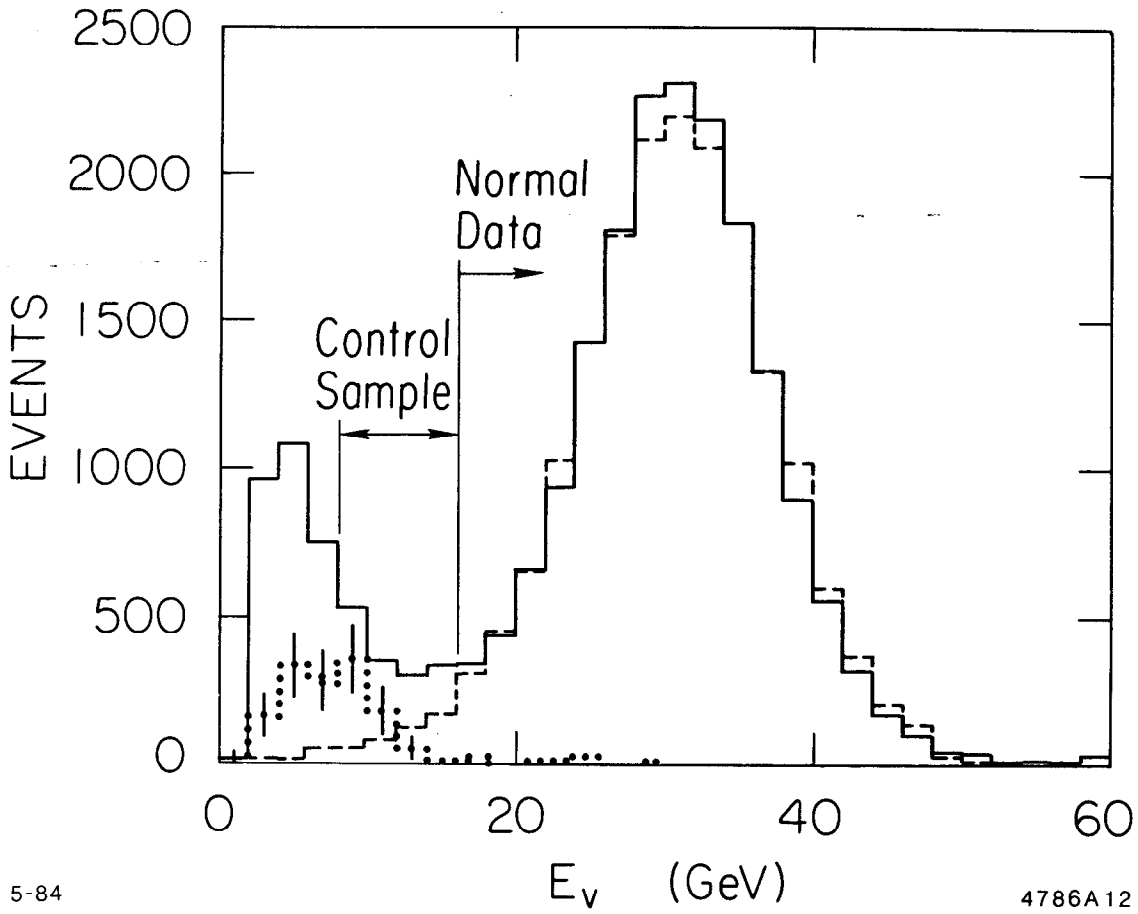
2500
2000
1500
1000
500
0
EVENTS
Normal
Data
Control
Sample
0
20
40
60
E_ν (GeV)
5-84
4786A12

Fig. 6

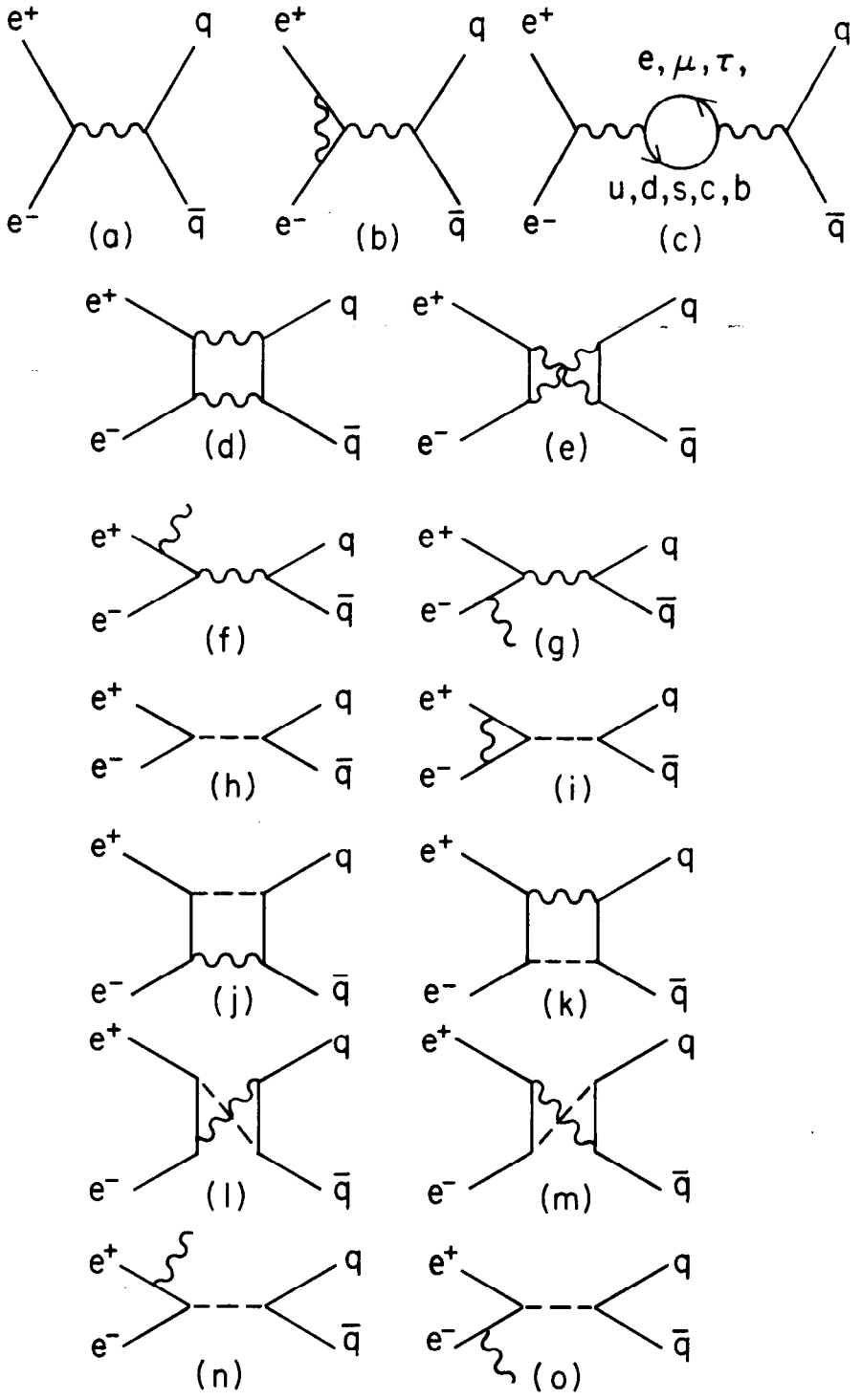

4-83

4512B23

Fig. 7